inorganics

MDPI

Review

Roles of Ti-Based Catalysts on Magnesium Hydride and Its Hydrogen Storage Properties

Chengshang Zhou [1,*], Jingxi Zhang [2,3], Robert C. Bowman, Jr. [4] and Zhigang Zak Fang [2]

[1] State Key Laboratory for Powder Metallurgy, Central South University, Changsha 410083, Hunan, China
[2] Department of Materials Science and Engineering, The University of Utah, Salt Lake City, UT 84112-0114, USA; jx-zhang@csu.edu.cn (J.Z.); zak.fang@utah.edu (Z.Z.F.)
[3] School of Metallurgy and Environment, Central South University, Changsha 410083, Hunan, China
[4] RCB Hydrides, LLC, 117 Miami Avenue, Franklin, OH 45005, USA; rcbjr1967@gmail.com
* Correspondence: chengshang.zhou@csu.edu.cn

Abstract: Magnesium-based hydrides are considered as promising candidates for solid-state hydrogen storage and thermal energy storage, due to their high hydrogen capacity, reversibility, and elemental abundance of Mg. To improve the sluggish kinetics of MgH_2, catalytic doping using Ti-based catalysts is regarded as an effective approach to enhance Mg-based materials. In the past decades, Ti-based additives, as one of the important groups of catalysts, have received intensive endeavors towards the understanding of the fundamental principle of catalysis for the Mg-H_2 reaction. In this review, we start with the introduction of fundamental features of magnesium hydride and then summarize the recent advances of Ti-based additive doped MgH_2 materials. The roles of Ti-based catalysts in various categories of elemental metals, hydrides, oxides, halides, and intermetallic compounds were overviewed. Particularly, the kinetic mechanisms are discussed in detail. Moreover, the remaining challenges and future perspectives of Mg-based hydrides are discussed.

Keywords: magnesium hydride; titanium-based hydride; catalysis; hydrogen storage properties

Citation: Zhou, C.; Zhang, J.; Bowman, R.C., Jr.; Fang, Z.Z. Roles of Ti-Based Catalysts on Magnesium Hydride and Its Hydrogen Storage Properties. *Inorganics* **2021**, *9*, 36. https://doi.org/10.3390/inorganics9050036

Academic Editor: Maurizio Peruzzini

Received: 31 March 2021
Accepted: 29 April 2021
Published: 6 May 2021

1. Introduction

Depletion of fossil fuels and changes in the global climate urge people to seek green, sustainable energy resources and high-efficiency energy systems. Hydrogen is one of the secondary energy solutions with high gravimetric energy density, high efficiency, and zero carbon emission [1]. However, the hydrogen economy relies on safe and mature technology to store hydrogen, which remains a great challenge [2]. Solid-state hydrogen storage using metal hydrides is considered to be a safe and efficient method in comparison to other storage technologies, such as compressed hydrogen gas or liquid hydrogen.

Among various solid-state hydrogen storage materials, magnesium hydride (MgH_2) is one of the metal hydrides that has been considered to be promising, due to its high storage capacity, abundant resources, and relative safety. MgH_2 was first prepared in 1912 [3], and was proposed that can be used as energy storage media since the 1960s [4]. MgH_2 is known for its high hydrogen storage content, up to 7.76 wt%. More importantly, Mg has a single and flat pressure plateau under desorption/absorption, and is an abundant resource in the crust, which makes it one of the most promising hydrogen storage materials comparing to others. Thus, Mg-based hydride is expected to play important roles in future hydrogen storage techniques. In past decades, research efforts have made significant progress on improving Mg-based hydrides in terms of thermodynamics, kinetics, and reversibility. The utilization of MgH_2 for "energy storage" relates to two aspects, namely, hydrogen storage (HS) [5] and thermal energy storage (TES) [6]. Despite the difference in material-level for HS and TES, both applications require Mg-based hydride

with fast hydrogen absorption and desorption rates. This leads to a large demand for studying catalysis in the Mg-H_2 system.

Due to the extensive research activities on Mg-based hydrides, a series of review papers have been published [7–14]. A comprehensive review by Yartys et al. [15] provides a historical overview as well as future perspectives. Recent reviews have covered various directions for Mg-based hydrogen storage, such as downsizing (nanostructuring) [7,10], catalysis and kinetics [7,16,17], and destabilization [18,19]. However, given the large volume of publications as well as many review papers on Mg-based hydride, it still lacks a review regarding a specific group of catalysts and responsible effects. Transition metals (TM)-based additives have been proved to be effective to enhance the hydrogen storage properties of MgH_2. Among different TM-based additives, Ti and its compounds are recognized as a group of promising additives, which have been widely investigated from many different aspects, including catalytic effects, catalysis mechanism, nano- and microstructures, and synthetic methods. In the past decades, much attention and many efforts were directed to this group of additives, with progress being continuously made. With a special emphasis on Ti-based catalysts, we intend to provide overviews of specific fundamental understanding and clear catalysis mechanisms for Mg-based material.

2. Fundamentals of the Mg-H_2 System

2.1. Crystal Structure

MgH_2 is a stoichiometric compound with a H/Mg atomic ratio of 1.99 ± 0.01 [20]. The Mg-H bond is an ionic type that is similar to alkali and alkaline earth metal hydrides [21]. MgH_2 with different types of structures can be synthesized by the reaction of magnesium with hydrogen under different conditions. β-MgH_2, which is stable at ambient pressure (1 bar) and room temperature, has a tetragonal TiO_2-rutile-type structure with space group $P4_2/mnm$ [22]. β-MgH_2 can be formed under moderate conditions during reversible hydrogen cycling. Nevertheless, MgH_2 has at least four high-pressure forms, and the corresponding crystal structure parameters are tabulated in Table 1. At high applied pressures exceeding 0.387GPa or milled under high energy, β-MgH_2 transforms into the orthorhombic γ-MgH_2 form with α-PbO_2-type structure [23]. Additionally, a subsequent phase transition from γ-MgH_2 to a modified-CaF_2-type structure was observed experimentally using in situ synchrotron diffraction when hydrogen pressure is above 3.84 GPa [24]. According to Varin et al., high energy ball-milling of MgH_2 produced γ-MgH_2 coexisted with nanocrystalline β-MgH_2. They suggested that the presence of the γ-MgH_2 phase contributed to reducing the hydrogen desorption temperature of MgH_2 [25].

Table 1. Optimized structural parameters, bulk modulus (B_0), and pressure derivative of bulk modulus (B'_0) for MgH_2 in ambient and high-pressure phases. (Reprinted with permission from ref. [22]. Copyright 2006 American Physical Society.)

Modification Structure Type	Unit Cell (Å) a	b	c	Positional Parameters	B_0 (GPa)	B'_0
β-MgH_2, TiO_2-rutile ($P4_2/_{mnm}$)	4.5176	4.5176	3.0206	Mg (2*a*): 0, 0, 0	45.00 ± 2	3.35 ± 0.3
γ-MgH_2, Modified CaF_2 ($Pa\bar{3}$)	4.6655	4.6655	4.6655	Mg (4*a*): 0, 0, 0	47.41 ± 4	3.49 ± 0.4
α-MgH_2, α-PbO_2 (P_{bcn})	4.5246	5.4442	4.9285	Mg (4*c*): 0, 0.3313[d], 1/4[d]	44.03 ± 2	3.17 ± 0.4
δ′-MgH_2, $AuSn_2$ (P_{bca})	8.8069	4.6838	4.3699	Mg (8*c*): (0.8823, 0.0271, 0.2790)	49.83 ± 5	3.49 ± 0.6

2.2. Thermodynamics of the Mg-H_2 System

The first experimental evaluation of the thermodynamics of the Mg-H_2 system was reported by Stampfer et al., showing the enthalpy of formation of MgH_2 to be −74.5 kJ/mol·H_2, and the entropy of formation is 136 J/K·mol·H_2 [20]. The thermodynamics parameters of the Mg-H_2 system have been reported, see Table 2. The pressure-composition-isotherm (PCI) method is commonly used to determine the enthalpy (ΔH) and entropy

(ΔS) of the Mg-H_2 system. By measuring a series of equilibrium pressures at various temperatures, ΔH and ΔS can be derived by Van 't Hoff relation.

Table 2. Thermodynamic parameters and energy storage properties of MgH_2 [26].

Thermodynamic Parameters	Values
Formation enthalpy, kJ/(mol·H_2)	−74.5
Formation entropy, J/(mol·H_2·K)	−135
Hydrogen Storage Capacity (Theoretical)	
Gravimetric capacity, wt%	7.6
Volumetric capacity, g/(L·H_2)	110
Thermal Energy Storage Capacity (Theoretical)	
Gravimetric capacity, kJ/kg	2204
Volumetric capacity, kJ/dm^3	1763

For on-board solid-state hydrogen storage, a thermodynamic window in the range of approximately 25–45 kJ/mol·H_2 is recognized for suitable metal hydride material [27]. Therefore, efforts have been directed to destabilize the MgH_2, or in other words, reducing the ΔH of MgH_2. It is expected that reducing ΔH can lower the working temperature for Mg-based hydride, which is crucial for on-board applications. Three typical approaches were proposed to destabilize MgH_2, namely, alloying, downsizing, and stress effect.

The alloying method refers to alloying other elements with Mg to form a new alloy or hydride compound with lower stability of its hydride. So far, alloying systems have been reported including Mg_2NiH_4 [28], Mg_2FeH_6, Mg_2CoH_5, Mg_2Cu [29], Mg(Al) [30], $Mg_{51}Zn_{20}$ [31], Mg_2Si [32], Mg(In) [33], Mg(Sn) [21], Mg(AgIn) [34], MgReNi [35], Mg_2M-xM_xH_y (M = Fe, Co, Ni), and so on. The principle is using a less-stable hydriding element A to form an Mg-A alloy. The energy diagram of the alloying method is illustrated in Figure 1. Since Mg-Ti is an immiscible system, Mg and Ti do not form an alloy. However, metastable Mg-Ti-H compounds have been reported. Kohta et al. [36–39] successfully synthesized Mg_xTi_{100-x} ($35 \le x \le 80$) alloys with hexagonal close-packed (HCP), face-centered cubic (FCC), and body-centered cubic (BCC) structures by ball milling. Vermeulen et al. [40] reported that Mg-Ti-H system has a very low plateau pressure (≈10^{-6} bar at room temperature). Additionally, it will have a higher plateau pressure and a reversible hydrogen storage capacity of more than 6 wt%, when forming ternary compositions with Al or Si.

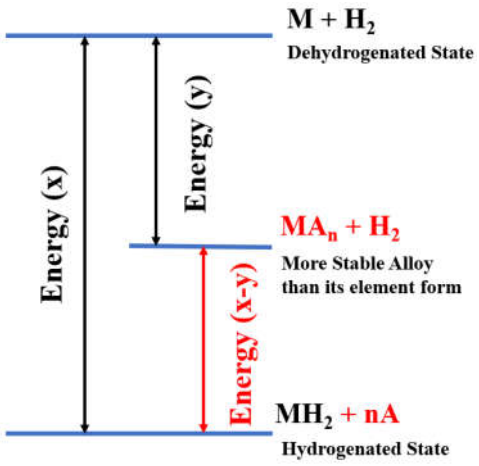

Figure 1. Schematic of destabilization process of a hydride MH using third element A. (Reproduced with permission from ref. [41]. Copyright 2016 Elsevier.)

Nano-sizing of Mg-based materials is not only a strategy to enhance kinetics, but also considered as an approach to destabilize MgH_2. It has attracted a great deal of effort in the

past decades, despite its effectiveness and feasibility remaining controversial. The influence of nano-sizing on pressure-temperature dependence as well as ΔH is given in Figure 2. Theoretically, nanosizing to hydrides introduces excessive free energy to bulk or coarse particles. The excessive free energy may originate from lattice distortion [42]. Sadhasivam et al. [8] summarized the dimensional effects of nanostructured Mg/MgH_2 materials. They reported that Mg/MgH_2 with a particle size <5 nm has improved hydrogen storage properties. However, a great challenge remains in synthesizing such fine particles as well as maintaining the nano-size after thermal cycling for Mg-based materials. According to [8], the 1-dimensional Mg nanowire shows a promising hydrogen storage property. However, the nanowire structure would collapse into nanoparticles after a few cycles. Additionally, it is reported that reducing magnesium hydride structure to nanosize induces the stress/strain effect, which has been reviewed by Zhang et al. [43] It was pointed out that the stress/strain applied on MgH_2 leads to lattice deformation and volume change, which endows the extra strain energy for MgH_2. The research of Berube et al. [44] supported this claim. They reported that a 15% reduction of the formation enthalpy of nanostructured MgH_2 can be achieved by the introduction of surfaces, grain boundaries, as well as the presence of γ-MgH_2. Recent reviews [8,45,46], have provided thoughtful introduction and discussion into the thermodynamic aspects.

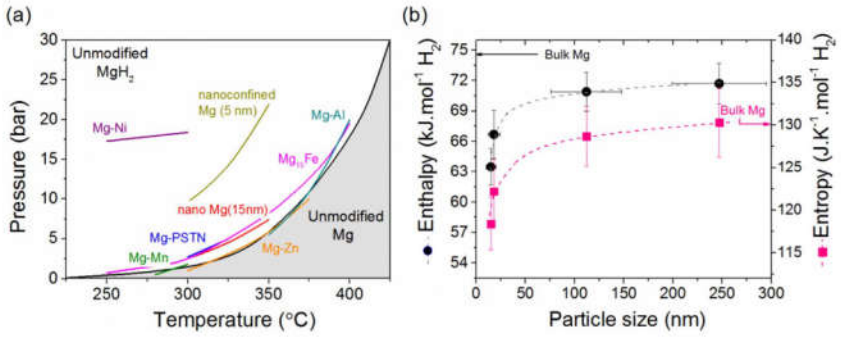

Figure 2. (**a**)Temperature dependence of the dissociation pressure of MgH_2 and associated evolution of such a dissociation pressure for various approaches investigated, and (**b**) evolution of ΔH and ΔS as a function of the particle size of Mg. (Reproduced with permission from ref. [47]. Copyright 2018 Elsevier.)

2.3. Kinetics

Kinetics for hydrogen storage materials is generally defined as the dynamic rate where hydrogenation and dehydrogenation take place in time. Kinetics measurements provide critical information on the rates of hydrogen uptake or release from Mg-based materials. It is necessary to be rather explicit when investigating hydrogenation and dehydrogenation kinetics. For pure Mg and MgH_2 in the conventional form of coarse powders, they demonstrate very sluggish kinetics for hydrogen absorption and release, usually requiring over 400 °C for the reverse reactions. The slow hydrogenation rate of Mg, as well as dehydrogenation rate of MgH_2, can be attributed to several intrinsic factors: dissociation of the hydrogen molecule, penetration of hydrogen through the surface, diffusion of hydrogen in the matrix, in addition to possible contamination in the sample environment.

For hydrogenation of Mg, dissociation of the hydrogen molecule on the Mg surface is often considered as a rate-limiting step. Table 3 summarizes the energies for hydrogen molecule dissociation on Mg and modified Mg surfaces. The reported values of hydrogen dissociation energy on the Mg surface are in the range of 0.4–1.15 eV (38.59–110.96 kJ/mol), which is higher than most transition metals, such as Ti, V, Ni, and Fe [48]. This means that a large energy barrier needs to be overcome for dissociation of H_2 on pure Mg (0001) surfaces [49]. Another intrinsic issue is the slow hydrogen diffusion rate in MgH_2. Figure 3 shows the geometry model of the reaction for an Mg/MgH_2 particle. Based on the model,

the hydride layer formed on the particle surface becomes the major barrier during hydrogenation, since the hydrogen atom diffusion rate in the hydride phase is much slower than that in the metallic phase. According to Spatz et al., the hydrogen diffusion coefficient (D_H) of MgH_2 is quite low (1.1×10^{-20} m^2/s at 305 K) [50]. Figure 4 shows that the D_H of MgH_2 is at magnitudes lower than the D_H of the Mg metal phase. It is also evident in this figure from the diffusion coefficient plots that most transition metals and their hydrides have D_H several magnitudes higher than the D_H of MgH_2.

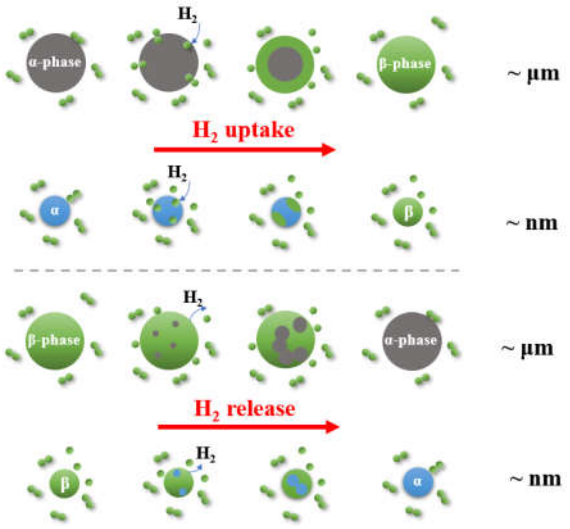

Figure 3. Schematic of the hydrogen absorption/desorption process in the MgH_2/Mg. (Reproduced with permission from ref. [47]. Copyright 2018 Elsevier.).

Table 3. Dissociation energy of hydrogen molecule on the surface of Mg. (Reproduced with permission from ref. [49]. Copyright 2008 AIP Publishing).

Metal	Dissociation Energy (eV)
Pure Mg	0.87, 0.40, 0.50, 1.15, 1.05, 0.95, 1.00
Ti-doped Mg	Null, negligible
Ni-doped Mg	0.06
V-doped Mg	Null
Cu-doped Mg	0.56
Pd-doped Mg	0.39
Fe-doped Mg	0.03
Ag-doped Mg	1.18

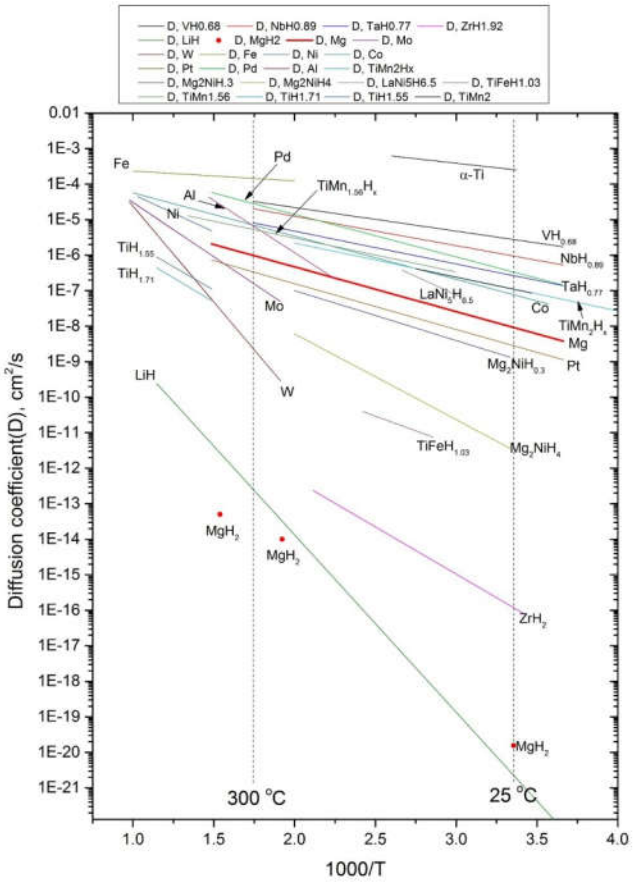

Figure 4. Hydrogen diffusion coefficients in different metals and hydrides. (Reprinted from ref. [51]. Copyright 2015 Chengshang Zhou.).

Catalytic doping and nanosizing of Mg-based systems have been considered as important methods to improve their kinetics. In general, the catalyst is defined as an agent which reduces the activation barrier without participating in the chemical reaction, as illustrated in Figure 5. A common consensus is that transition metals (TM) and their compounds are effective catalysts. These catalysts can be doped into Mg/MgH_2 material by different synthetic approaches. Most TM catalysts are effective in both hydrogenation and dehydrogenation reactions. The roles of different Ti-based catalysts and the underlying mechanism will be reviewed in the following section.

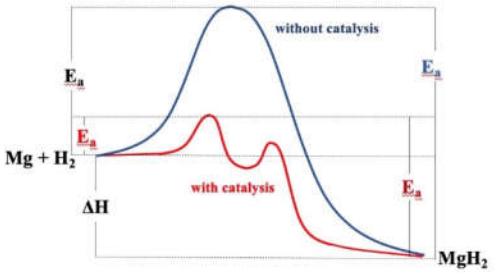

Figure 5. Representation of the kinetic barrier of the reaction and lowering the activation energy (E_a) using a catalyst. (Reprinted from ref. [52]. Copyright 2018 MDPI.).

Downsizing MgH_2 to nano-scale is also shown to be effective to improve the kinetics. It is believed that nano-sizing can enhance kinetics by the creation of a large amount of fresh surface, shortening hydrogen diffusion, and promoting nucleation of the hydride/metal phase [12]. It is noteworthy that a combination of nanosizing and catalytic doping is usually realized during synthesis. For example, using a high-energy ball milling technique, co-milling MgH_2 with transition metal powder could produce a nanocomposite with nano-size microstructure and homogeneously doped catalyst particles.

3. Catalytic Effects

3.1. Transition Metals Catalysts

Among various additives for improving Mg-based materials, TM catalysts have been intensively investigated. Interestingly, most of the transition metals and their compounds are found to be effective as both hydrogenation and dehydrogenation catalysts. In general, 1–5 at.% addition of TM catalyst leads to dramatic improvement while the hydrogen storage capacity is not sacrificed significantly. Research efforts have been directed to investigate the effectiveness of various TM-based catalysts. Table 4 compiles the reported results from Ti-based additive-enhanced MgH_2 systems as well as corresponding synthetic approaches and kinetic behaviors.

Early work by Liang et al. [53] evaluated the catalytic effects of 3d-TM elements (Ti, V, Mn, Fe, and Ni) on the reaction kinetics of ball-milled catalyzed MgH_2 (see Figure 6). The MgH_2-Ti composite showed superior hydrogen desorption/absorption kinetics, exhibiting the best desorption kinetics at 573 K, followed in order by V, Fe, Ni, and Mn. The activation energies (E_a) of MgH_2-Ti, MgH_2-V, MgH_2-Mn, MgH_2-Fe, and MgH_2-Ni are calculated to be 71.1 kJ/mol, 62.3 kJ/mol, 104.6 kJ/mol, 67.6 kJ/mol, and 88.1 kJ/mol, respectively, which are significantly reduced compared to that of the ball-milled pure MgH_2 (120 kJ/mol). It was indicated that the TM catalysts could drastically improve the kinetic properties of MgH_2, among which Ti-catalyzed MgH_2 shows superior performance. Rizo-Acosta et.al. [54] compared hydrogenation properties of MgH_2 with the addition of early transition metals (Sc, Y, Ti, Zr, V, and Nb). As shown in Figure 7a,b, their results indicated that full reactions finished within less than 120 min in all cases and the hydrogen absorption rate increased along the sequence Y < V < Ti < Nb < Sc < Zr. However, an apparent degradation was observed when the cycling number increases. Interestingly, this evolution is less pronounced in the Ti-doped system, as shown in Figure 7c, which was attributed to the lattice mismatch between Mg and TiH_2 hydride that limits Mg grain growth. Among all cases, MgH_2-TiH_2 nanocomposite presented the best cycling properties with a reversible capacity of 4.8 wt% after 20 cycles and the reaction time arbitrarily limited to 15 min.

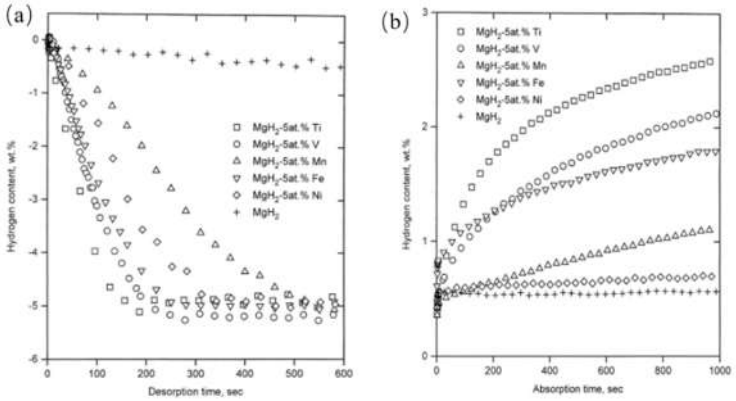

Figure 6. Hydrogen desorption curves ((**a**), desorption pressure of 0.015 MPa, 573 K) and absorption curves ((**b**), absorption pressure is 1.0 MPa, 302 K) of Mg–Tm composites. (Reproduced with permission from ref. [53]. Copyright 1999 Elsevier.).

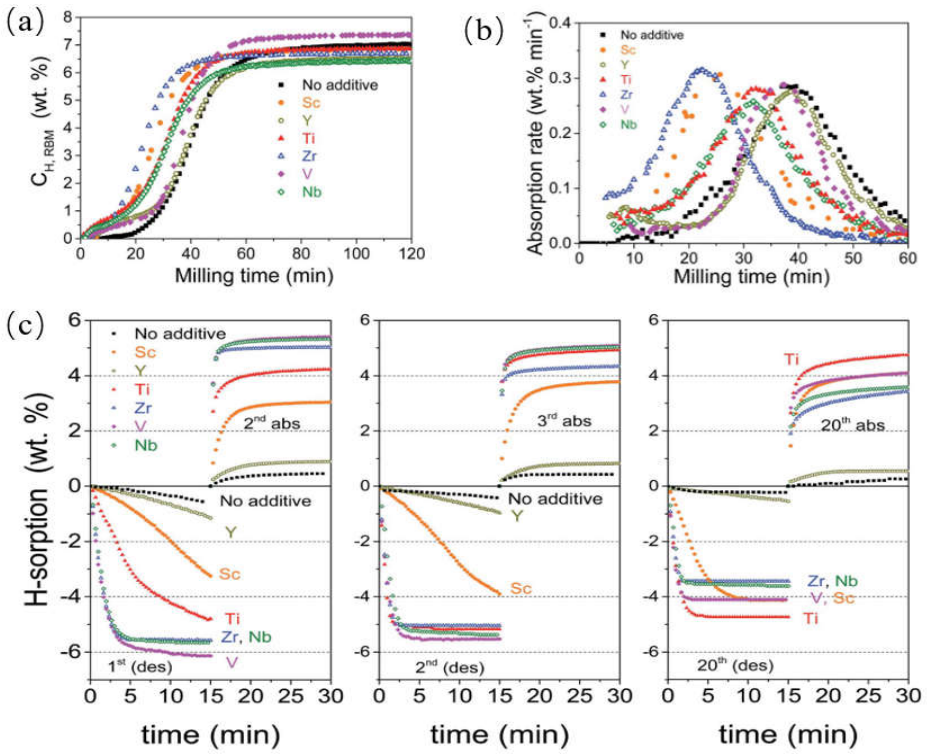

Figure 7. (**a**) Hydrogen uptake curves of 95Mg-5ETM powder mixtures during reactive ball milling synthesis; (**b**) the corresponding absorption rates (derivative curves of a); and (**c**) hydrogen sorption curves at 573 K of MgH_2-$ETMH_x$ NCs for different sorption sweeps. (Reproduced from ref. [54]. Copyright 2019 RSC.).

Table 4. Hydrogen storage properties of Mg with various types of Ti-based catalysts.

Materials	Synthetic Methods	Hydrogen Storage Properties				Reference
		Desorption Kinetics	Ea_{des} (kJ/mol)	Absorption Kinetics	Ea_{abs} (kJ/mol)	
Titanium/Titanium Hydrides						
Mg-2%Ti	Inert gas condensation	Des: 4.50%/320 °C/0.2 bar/25 min		Abs: 4.80%/320 °C/8 bar/21 min		[55]
MgH_2 + 2 at% Ti	Ball milling (argon)	Des: 6.32 wt%/623 K/35 kPa/0.5 h		Abs: 6.32 wt%/623 K/2000 kPa/4 min		[56]
	Cold rolling (5 times, air)	Des: 6.00 wt%/623 K/35 kPa/0.5 h		Abs: 5.70 wt%/623 K/2000 kPa/4 min		
MgH_2-4 mol% Ti	Ball milling	Des: 1.10%/573 K/2 MPa/5 min		Abs: 6.40%/573 K/2 MPa/5 min		[57]
MgH_2-5 at% Ti	Ball milling	Des Temperature: 235.6 °C	70.11			[58]
MgH_2-5 at% Ti	Ball milling	Des: 5.50%/523 K/0.015 MPa/20 min	71.1	Abs: 4.20%/373 K/1.0 MPa/15 min		[53]
MgH_2-5 at% Ti	Ball milling	Des: 5.20%/573 K/0.03 MPa/15 min		Abs: 6.70%/ 573 K/0.8 MPa/15 min		[54]
Mg-5% Ti	Chemical vapor synthesis		104			[59]
Mg-14 at% Ti	Gas phase condensation		35		52	[60]
Mg-22 at% Ti			31		47	
MgH_2-15% Ti	Ball milling	Des: 0.12%/573 K/1 bar/60 min		Abs: 3.48%/573 K/12 bar/60 min		[61]
$Mg_{0.9}Ti_{0.1}$	Ball milling		76	Abs: 6.62% (after milling)		[62]
$Mg_{0.75}Ti_{0.25}$	Ball milling		88	Abs: 6.18% (after milling)		
$Mg_{0.5}Ti_{0.5}$	Ball milling		91	Abs: 5.21% (after milling)		
MgH_2-20% Ti	Ball milling		72 ± 3			[63]
MgH_2-coated Ti	Ball milling	Des: 5.00%/250 °C/15 min (TPD) Des Temperature: 175 °C				[64]
$Mg_{83.5}Ti_{16.5}$	Inert gas condensation	Des: 2.50%/300 °C/0.15 bar/2 min		Abs: 2.20%/300 °C/9 bar/1 min		[65]
15Mg-Ti	Chemical method				72.2	[66]
MgH_2-4 mol% TiH_2	Ball milling	Des: 0.70%/573 K/2 MPa/5 min		Abs: 6.10%/573 K/2 MPa/5 min		[57]
MgH_2-5 at% TiH_2	Ball milling	Des: 5.80%/270 °C/0.12 bar/10 min Des Temperature: 235.5 °C	67.24	Abs: 2.70%/25 °C/1 bar/250 min		[58]
10MgH_2-TiH_2	Ball milling		73			[67]
7MgH_2-TiH_2	Ball milling		71			[68]
4MgH_2-TiH_2	Ball milling		68			[68]
MgH_2-10 mol% TiH_2	Ball milling			Abs: 5.70%/240 °C/2 MPa/200 s	16.4	[69]

MgH_2-10% TiH_2	Ball milling				24.2	[70]
MgH_2-10% TiH_2	Ball milling				17.9	[71]
Mg-9.2% $TiH_{1.971}$-3.7% $TiH_{1.5}$	Ball milling	Des: 4.10%/573 K/100 Pa/20 min	46.2	Abs: 4.30%/298 K/4 MPa/10 min	12.5	[72]
$Mg_{0.65}Ti_{0.35}D_{1.2}$	Ball milling		17			[73]
		Titanium Oxides				
MgH_2-10% TiO_2	Ball milling	Des: 6.00%/300 °C/vacuum/20 min		Abs: 6.00%/300 °C/0.84 MPa/5 min		[74]
Mg-20% TiO_2	Reactive ball milling	Des: 4.40%/350 °C/1 bar/8.5 min		Abs: 3.80%/350 °C/20 bar/2 min		[75]
MgH_2-6% TiO_2	Ball milling		145.8 ± 14.2			[76]
MgH_2 + 10% TiO_2	Ball milling	Des Temperature: 200 °C	75.50			[77]
		Titanium Halides				
MgH_2-10% TiF_4	Ball milling	Des Temperature: 216.7 °C	71	(Des: 6.6%)		[78]
MgH_2-10% TiF_4	Ball milling (2 h, argon)	Des Temperature: 154 °C	70			[79]
MgH_2 + 10% TiF_4	Ball milling	Des Temperature: 150 °C	70			[77]
MgH_2-4 mol% TiF_3	Ball milling	Des: 4.50%/573 K/2 MPa/5 min		Abs: 5.10%/573 K/2 MPa/5 min		[57]
MgH_2-4 mol% $TiCl_3$	Ball milling	Des: 3.70%/573 K/2 MPa/5 min		Abs: 5.30%/573 K/2 MPa/5 min		[57]
MgH_2-7% $TiCl_3$	Ball milling	Des temperature: 274 °C	85			[80]
		Titanium Alloys				
MgH_2-5a% TiAl	Ball milling	Des: 4.90%/270 °C/0.12 bar/10 min Des Temperature: 219.6 °C	65.08	Abs: 2.50%/25 °C/1 bar/250 min		[58]
MgH_2-5 a% Ti_3Al	Ball milling	Des Temperature: 232.3 °C	70.61			[58]
$Mg_{85}Al_{7.5}Ti_{7.5}$	DC-magnetron co-sputtering	Des: 5.30%/200 °C/vacuum/20 min		Abs: 5.60%/200 °C/3 bar/0.5 min		[81]
$Mg_{0.63}Ti_{0.27}Si_{0.10}D_{1.1}$	Ball milling		27			[73]
MgH_2-5 at%TiNi	Ball milling	Des Temperature: 242.4 °C	73.09			[58]
15Mg-Ti-0.75Ni	Chemical method				63.7	[66]
$Mg_{0.63}Ti_{0.27}Ni_{0.10}D_{1.3}$	Ball milling		21			[73]
MgH_2-5at%TiNb	Ball milling	Des: 5.90%/27 °C/0.12 bar/10 min Des Temperature: 231.3 °C	71.72	Abs: 2.80%/25 °C/1 bar/250 min		[58]
MgH_2-5at% Cr-5a% Ti	Film	Des: 6.00%/200 °C/5 mbar/25 min		Abs: 6.20%/200 °C/3 bar/10 min		[82]
MgH_2-7 at% Cr-13 at% Ti	Film	Des: 5.00%/200 °C/5 mbar/25 min		Abs: 5.60%/200 °C/3 bar/10 min		
MgH_2-5 at% TiFe	Ball milling	Des: 5.20%/270 °C/0.12 bar/10 min Des Temperature: 237.7 °C	72.63	Abs: 3.00%/25 °C/1 bar/250 min		[58]
MgH_2-5% FeTi	Ball milling			Abs: 2.30%/150 °C/2 MPa/5 min	21	[83]
MgH_2-5 at% $TiMn_2$	Ball milling	Des: 4.80%/270 °C/0.12 bar/10 min Des Temperature: 219.7 °C	74.22	Abs: 3.20%/25 °C/1 bar/250 min		[58]

MgH_2-10% $TiMn_2$	Ball milling				22.6	[70]
MgH_2-5% VTi	Ball milling			Abs: 3.30%/150 °C/2 MPa/5 min	10.4	[83]
$Mg_{87.5}Ti_{9.6}V_{2.9}$	Hydrogen plasma metal reaction	Des: 4.00%/300 °C/1 mbar/5 min	73.8	Abs: 4.80%/200 °C/40 bar/5 min	29.2	[84]
MgH_2-5 at% TiVMn	Ball milling	Des: 5.70%/270 °C/0.12 bar/10 min Des Temperature: 216.7 °C	85.20	Abs: 3.00%/25 °C/1 bar/250 min		[58]
Multiple Catalysts						
Mg-10% Ti-10% Pd	Ball milling		114 ± 4			[85]
Mg-$TiH_{1.971}$-$TiH_{1.5}$-$ZrH_{1.66}$	Arc melting		36.6		21.2	[86]
$Mg_{0.9}Ti_{0.1}$ + 5% C	Ball milling		88	Abs: 6.43% (after milling)		[62]
MgH_2-6% $NiTiO_3$	Ball milling		74 ± 4			[87]
MgH_2-6% $CoTiO_3$	Ball milling		100 ± 2			
MgH_2-10 mol% TiH_2-6 mol% TiO_2	Ball milling		118			[88]
MgH_2-5% VTi-CNTs	Ball milling			Abs: 5.10%/150 °C/2 MPa/5 min	10.2	[83]
MgH_2-5% FeTi-CNTs	Ball milling			Abs: 0.60%/150 °C/2 MPa/5 min	65.5	[83]
MgH_2-10% Ni-TiO_2	Ball milling	Des: 6.50%/265 °C/0.02 bar/7 min	43.7 ± 1.5	Abs: 5.00%/100 °C/60 bar/7 min		[76]
MgH_2-4% Ni-6% TiO_2	Ball milling		91.6 ± 8.5			[76]
MgH_2-10% Co-TiO_2	Ball milling	Des: 6.20%/250 °C/0.02 bar/15 min	77	Abs: 4.24%/100 °C/60 bar/10 min		[89]

Zhou et al. [90] prepared 49 additive-doped MgH_2 samples by ultra-high-energy-high-pressure ball milling, in order to conduct a comprehensive survey on a wide range of additives and corresponding dehydrogenation temperatures of the catalyzed MgH_2. The plot of the Thermogravimetric Analysis (TGA) dehydrogenation temperatures is shown in Figure 8, indicating that the additives containing the IV-B and V-B group elements are the most effective catalysts while the VII-B (Mn), VIII-B (Fe, Co, and Ni) groups show moderate catalytic effects. Besides, Ti and its compounds are more effective compared to those catalysts based on heavier elements (Zr, ZrH_2, ZrO_2, and Ta) in the same periodic group.

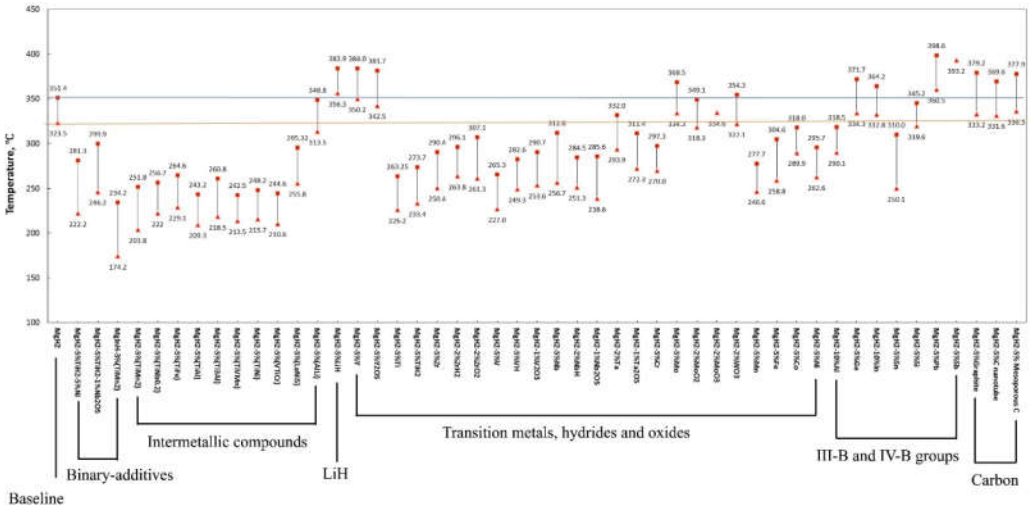

Figure 8. Effect of various additives on dehydrogenation temperatures of MgH_2. (Reprinted with permission from ref. [90]. Copyright 2015 Elsevier.).

Cui et al. [91] synthesized micro-sized Mg particles coated with nano-sized TM catalyst, showing that the nano-coating of TM on the Mg/MgH_2 surface is more effective than co-ball-milling of Mg with TMs. The authors also suggested that the catalytic improvement on dehydrogenation kinetics can be ranked as Mg-Ti, Mg-Nb, Mg-Ni, Mg-V, Mg-Co, and Mg-Mo, and the hydrogenation kinetics is in a sequence of Mg-Ni, Mg-Nb, Mg-Ti, Mg-V, Mg-Co, and Mg-Mo.

It has been recognized that early transition metals (ETM) belong to the group of most effective catalysts. Despite some discrepancies in reported data, Ti-based catalysts, involving not only elemental Ti but also Ti hydrides, oxides, halides, and intermetallic compounds have shown great benefits in improving the hydrogen storage properties of MgH_2. In-depth investigations of Ti-based catalysts are also beneficial for understanding the catalysis mechanism for the Mg-H_2 system.

3.2. Catalytic Effects of Ti-Based Compounds

A large number of Ti-based catalysts have been explored for enhancing the hydrogen storage properties of MgH_2. Early attempts using elemental Ti powder to ball-mill with MgH_2 received encouraging results [53]. Soon, researchers found that TiH_2 powder additive is very effective as well. Lu et al. [92] reported exceptional room temperature hydrogenation properties of MgH_2-0.1TiH_2 material prepared by ultra-high-energy-high-pressure (UHEHP) ball milling. Liu et al. [72] studied the effects of two different Ti hydrides ($TiH_{1.971}$ and $TiH_{1.5}$) on the hydrogenation kinetics of Mg. It pointed out an important fact that elemental Ti can easily react with hydrogen to form various Ti hydrides under certain temperatures and hydrogen pressures. During the reverse hydrogen reaction, the following equations can be summarized:

$$Mg + Ti + H_2 \rightarrow Mg + TiH_{1.971} \quad (1)$$

$$Mg + TiH_{1.5} + TiH_{1.971} + H_2 \rightarrow MgH_2 + TiH_{1.5} + TiH_{1.971} \quad (2)$$

$$MgH_2 + TiH_{1.5} + TiH_{1.971} \rightarrow Mg + TiH_{1.5} + TiH_{1.971} + H_2 \quad (3)$$

According to the Mg-Ti phase diagram, neither Ti nor Ti hydrides are immiscible with Mg or MgH_2 phases. Furthermore, no ternary Mg-Ti hydride exists in the phase diagram. However, under a metastable condition, it is possible for Ti to dissolve into Mg and form a solid solution. Ponthieu et al. [93] reported Ti solubility in β-MgD_2 up to 7 at.%, and Mg solubility in TiD_2 up to 8%, which suggested shortened D-diffusion path due to the introduction of TiD_2. An Nuclear Magnetic Resonance (NMR) study of MgD_2/TiD_2 composite found lattice coherent fluorite (fcc) structured TiD_2 and MgD_2, which is expected to be a fast H-diffusion pathway to accelerate the kinetics. [94]

Another focus is discovering a novel metastable Mg-Ti-H hydride with a new structure. Kyoi et al. [95] synthesized Mg_7-Ti-H FCC hydride using a high-pressure anvil cell. Asano and Akiba reported the ball-milling synthesis of a series of Hexagonal Closest Packed (HCP), Face-centered Cubic (FCC), and Body-centered Cubic (BCC) Mg_xTi_{100-x} alloys, and Mg-Ti-H FCC hydride phases with chemical formulae of $Mg_{40}Ti_{60}H_{113}$ and $Mg_{29}Ti_{71}H_{57}$. These ternary hydrides had lower stabilities in comparison to MgH_2 and thus show lower desorption temperatures.

TiO_2 was considered an effective catalyst. Wang et al. [75] prepared ball-milled Mg-TiO_2 and showed good hydrogenation and dehydrogenation kinetics. For the past two decades, however, the investigation of oxide catalysts paid more attention to Nb_2O_5, since it seems to be more efficient among transition metal oxides [96]. Actually, doping of TiO_2 would present a similar effect comparing to the Nb_2O_5 catalyst. As suggested by Pukazhselvan et al. [97], TiO_2 can be partially reduced to a lower $3^+/2^+$ state (TiO and Ti_2O_3). The presence of $Mg_xTi_yO_{x+y}$ oxide was also suspected, but no direct support was seen by X-ray Diffraction (XRD) results. More recently, Zhang et al. [98] showed good catalytic activity of carbon-supported nanocrystalline TiO_2 (TiO_2@C). It was reported that the dehydrogenation temperature of MgH_2-10 wt%TiO_2@C can be lowered to 205 °C and hydrogen uptake took place at room temperature. Berezovets et al. [99] reported that the Mg-5 mol% $Ti_4Fe_2O_x$ was able to absorb hydrogen even at room temperature after hydrogen desorption at 300–350 °C and its cycling stability could be substantially improved by introduction of 3 wt% graphite into the composite.

Ti halides have been reported to offer a positive effect on the kinetics of MgH_2. TM fluorides usually present superior catalytic effects and satisfactory kinetics. Malka et al. [80] reported the catalytic effects of a group of TM fluorides (FeF_2, NiF_2, TiF_3, NbF_5, VF_4, ZrF_4, CrF_2, CuF_2, CeF_3, and YF_3) on the kinetics of MgH_2. The best catalysts for magnesium hydride decomposition were selected to be ZrF_4, TaF_5, NbF_5, VCl_3, and $TiCl_3$. In another investigation by Jin et al. [100], it was suggested that TiF_3 and NbF_5 showed better effects over other TM fluorides. It was found that the hydride, for example, TiH_2, formed after co-milling MgH_2 with the fluorides, with an in situ reaction described as follows:

$$3MgH_2 + 2TiF_3 \rightarrow 3MgF_2 + 2TiH_2 + H_2 \quad (4)$$

Moreover, Wang et al. [101] conducted a comparison study on the elemental Ti, TiO_2, TiN, and TiF_3 catalyzed MgH_2 materials, showing that TiF_3 had the strongest catalytic effect among them.

Ti-based intermetallics as catalysts have been receiving active attention in recent years. Early researchers used TiFe [102], $(Fe_{0.8}Mn_{0.2})Ti$ [103], Ti_2Ni [104], and $TiMn_{1.5}$ [105] additives to improve hydrogen storage properties of MgH_2, showing that all these intermetallics were effective catalysts. Interestingly, some Ti-based intermetallics themselves, including TiFe and $TiMn_{1.5}$, are known as hydrogen storage alloys. Zhou et al. [58] conducted a systematic investigation focusing on a series of Ti-based intermetallic catalysts

(i.e., TiAl, Ti3Al, TiNi, TiFe, TiNb, TiMn2, and TiVMn). The results found that $TiMn_2$-doped Mg demonstrated extraordinary hydrogen absorption capability at room temperature and 1-bar hydrogen pressure while its apparent activation energy is 20.59 kJ/mol·H_2. The strong catalytic effect of $TiMn_2$ is also confirmed by another experimental work by El-Eskandarany et al. [106,107] and first principles calculation by Dai et al. [108].

4. Synthetic Approaches

The synthesis methods of Mg-based hydrides have a great impact on their hydrogen storage properties. With expanding research scope of hydrogen storage materials, there are emerging preparation methods in recent years. Many hydrogen storage alloys can be prepared by physical methods, including ball milling [109], induction melting [110], arc melting [111], et cetera. Complex hydrides are usually prepared by chemical methods, such as organic synthesis, hydrothermal method, and solvothermal method [112]. However, conventional high-temperature preparations such as sintering or melting have been largely restricted due to the low melting temperature and high vapor pressure of magnesium [15]. Widely-used methods for Mg-based hydride preparation include ball milling, thin film deposition, and chemical methods.

4.1. Ball Milling

Ball milling is a mechanical method that grinds metal or alloy powder into extremely fine powders [113]. During ball milling, the collision between powder particles and grinding balls will generate localized high pressure and cold welding of powder particles repeatedly, which leads to interdiffusion and alloying between different elements to produce hydrides with nano-size structure [114–116]. By technical categorizing, there are mainly four kinds of high-energy ball-milling techniques to prepare Mg-based hydride: agitator [117], shaker/vibration type mills [118], planetary mill [119], and uni-ball mill [120]. The ball milling technique is quite effective to improve the hydrogen storage properties of magnesium-based alloys due to the following reasons. First, the native oxide layer can be broken during ball milling, and thus a large number of fresh surfaces is created [121,122]. Second, defects and grain boundaries can be produced during the ball milling process, which provides channels for bulk hydrogen diffusion [123]. Third, reduced grain size accelerates the diffusion of hydrogen atoms inside grains [124,125]. Fourth, ball milling of magnesium in hydrogen gas resulted in the formation of a mixture of β-MgH_2 and γ-MgH_2, which can destabilize the MgH_2 system, reduces H_2 desorption temperature, and improves the desorption kinetics [126,127]. Last, the defects and strain generated during ball-milling usually disappear after cycling the hydride, which may raise a concern about the kinetic degradation. However, several cycling studies observed that the high-temperature kinetics (~300 °C) maintained good stability, yet the low-temperature hydrogenation kinetics suffered a severe degradation after hydrogen cycles [128–130].

4.2. Thin Film Deposition

The thin-film deposition method can prepare doped Mg-based material with one dimension in the range of a few atoms to micrometers. It can be divided into two categories, physical vapor deposition (PVD) and chemical vapor deposition (CVD) coating systems. PVD is an atomistic deposition processes in which materials are vaporized from a solid or liquid source and then condensed onto the substrate [131]. Using PVD processes, Ti and other elements can be added into Mg to form the Mg-Ti-H system which can reduce the stability of MgH_2. Gremaud et al. [132] prepared Mg-Ni-Ti ternary alloy films, showing that the enthalpy of absorption/dehydrogenation of $Mg_{0.69}Ni_{0.26}Ti_{0.05}$ film reduced to 40 kJ/mol·H_2, as shown in Figure 9.

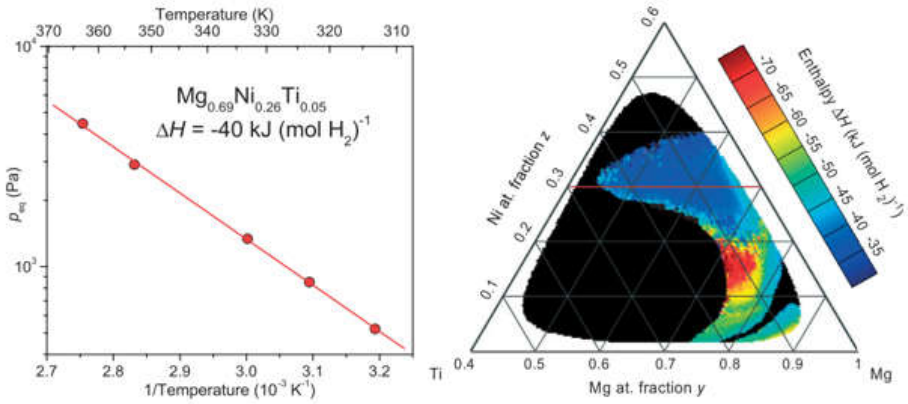

Figure 9. Diagram of enthalpy change of $Mg_{0.69}Ni_{0.26}Ti_{0.05}$ film and $Mg_yNi_zTi_{1-y-z}$ gradient film. (Reproduced with permission from ref. [132]. Copyright 2007 John Wiley and Sons.).

CVD is a coating process using a thermally induced vapor phase chemical reaction to deposit matter on a substrate surface, which provides great versatility for synthesizing both simple and complex compounds with relative ease at generally low temperatures [133]. This method is favorable for large-scale production because of its simple equipment, easily controlled reaction conditions, high purity, and narrow particle size distribution of products. Different shapes of crystals with different compositions were prepared by CVD at different temperatures and pressures, as shown in Figure 10, which might support the mass production of nano- and micro-sized MgH_2/Mg using hydrogen. Another approach to improve the hydrogen storage properties of Mg is by forming an alloy with other elements. For example, 1.5 μm thick Mg-Al-Ti, Mg–Fe–Ti, and Mg-Cr-V ternary alloy films showed remarkable kinetics at 200 °C [81,134].

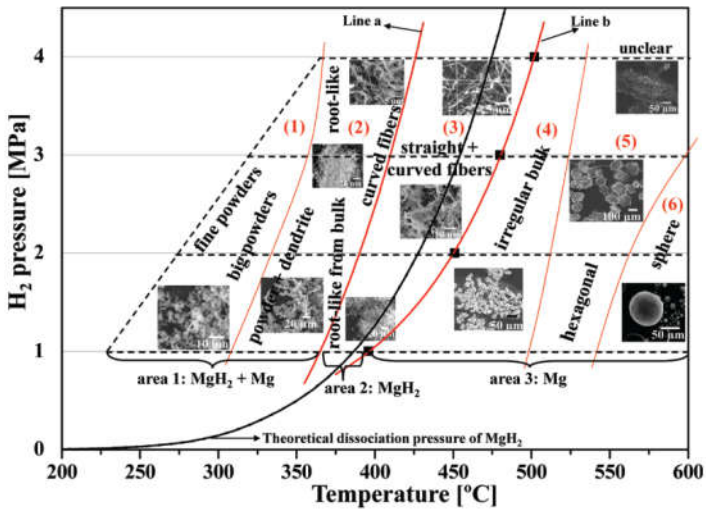

Figure 10. Simplified morphology and composition distributions of the deposited products at different deposition temperatures and H_2 pressures plotted in the P-T diagram of MgH_2 [135]. Copyright 2010 ACS Publications.

4.3. Chemical Methods

MgH_2 and doped Mg-based hydrides can also be synthesized by a chemical reaction from organic compounds. Chemical reduction to prepare Mg-based material nanoparticles is one of the bottom-up approaches with several advantages, including morphology control, easy separation, facile post-synthesis modifications, stable nanoparticles, and ease

of scaling up [136]. In the last two decades, molecular magnesium hydride chemistry has received a major boost from organometallic chemists with a series of structurally well-characterized examples [137]. Norberg et al. [138] reported that the density of defect sites of Mg nanocrystals is increased through the low-temperature reduction, which provides a simple route to enhance H_2 sorption kinetics dramatically. Mg nanoparticles synthesized by chemical reduction in solution usually have an irregular shape, with particle lengths/widths ranging from 7 to 60 nm. For a typical synthesis routine, Ti-catalyzed MgH_2 nanocrystalline was obtained from the reaction using Mg powder, anthracene, anhydrous tetrahydrofuran (THF) solution, and ethyl bromide, according to Equations (5)–(7) [139]. The nanocrystalline material consists of 89 wt% for the dominant β-MgH_2 phase and 11 wt% for γ-MgH_2, which surprisingly obtains γ-MgH_2 under relatively mild conditions (hydrogenation reaction at room temperature and under 8 MPa hydrogen pressure) [122].

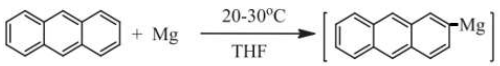

(5)

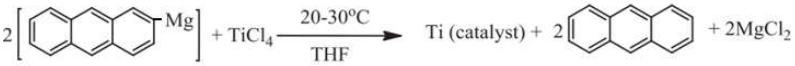

(6)

(7)

5. Mechanisms of Catalysis

Understanding the catalysis is critical to improving hydrogen absorption and desorption kinetics for Mg-based systems. Based on the understanding of the hydrogen reaction in the metal-hydrogen system [140], the hydrogenation of metal should go through the following five steps: (1) Physisorption of the H_2 molecule, (2) dissociation of the H_2 molecule, (3) surface penetration of H atoms, (4) diffusion of H atoms in the host lattice, and (5) hydride formation at metal/hydride interface, as shown in Figure 11. For the dehydrogenation reaction, a hydride particle could go through the following steps: (1) Hydride decomposition, (2) diffusion of hydrogen atom, (3) surface penetration, (4) recombination to hydrogen molecule, and (5) desorption to the gas phase. Either hydrogen absorption or desorption should be controlled by a rate-limiting step while other steps are likely in equilibrium.

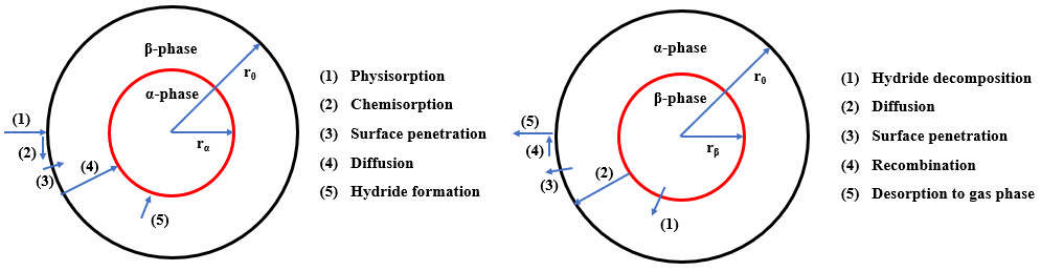

Figure 11. Reaction partial steps for the absorption (**left**) and desorption (**right**) of hydrogen by a spherical metal/hydride powder particle. (Reproduced with permission from ref. [140]. Copyright 1996 Elsevier).

However, the rate-controlling mechanisms in hydrogenation and dehydrogenation may not necessarily be the same. The physisorption of a H_2 molecule on a metal surface needs a very low activation energy, so it is generally not considered a limiting step. The rest of the steps can be rate-limiting which is worthy of discussion. For dehydrogenation, steps 1, 2, and 3 (illustrated in Figure 11) can be considered as possible rate-limiting steps. Note that the hydrogen atoms should diffuse across the metal phase, in which the diffusion coefficient is much higher compared to that in the hydride phase. Moreover, the

dehydrogenation has a H_2 recombination step instead of dissociation. The recombination of H atoms into a molecule does not have an energy barrier to overcome [141]. From these aspects, it seems reasonable that the kinetic barrier of dehydrogenation could be lower than that of hydrogenation. However, dehydrogenation is an endothermic reaction whereas hydrogenation is exothermic, which means the hydrogenation of Mg is favored in respect of thermodynamics. These fundamental differences may change the activation barrier and lead to different reaction behaviors.

5.1. Hydrogen Dissociation

Both theoretical calculation and experimental work have suggested that a large energy barrier needs to be overcome when hydrogen dissociates on a pure Mg surface. A density functional theory (DFT) study by Du et al. [142] shows that the hydrogen dissociation activation barrier will decrease from 1.051 eV for a pure Mg(0001) surface to 0.103 eV and 0.305 eV for Ti-doped and Pd-doped Mg(0001) surfaces, respectively. Another DFT work conducted by Yao et al. [143] reported the energy barrier for molecular hydrogen dissociation on the Mg surface to be 1.15 eV. The calculated activation energies for hydrogen dissociation on V and Ti atoms are 0.201 eV and 0.103 eV, respectively. Pozzo et al. [48] calculated that the energy for hydrogen dissociation on pure Mg(0001) is as high as 0.87 eV and Mg-Ti, Mg-V, Mg-Zr, and Mg-Ru have nearly zero dissociation barrier. In addition, nanosized metal surfaces may provide additional promotion for hydrogen dissociation, due to the increases of metal surface area and a number of steps, kinks, and corner atoms [12].

Once the hydrogen molecules dissociate into atoms on the surface, the obstacle may still exist to prevent transferring hydrogen atoms from catalytic sites into bulk. The so-called "hydrogen spillover" mechanism may play the role in Mg-TM catalyzed systems [83]. Hydrogen spillover refers to the surface migration of activated hydrogen atoms from a catalytic particle onto the matrix. This phenomenon has been intensively studied in catalysis science. However, hydrogen spillover in a catalyzed Mg-based system and migration is challenging to observe so it still lacks direct evidence.

According to Sabatier's principle, the catalyst for dehydrogenation/hydrogenation reactions should not bond with hydrogen too strongly or too weakly. This leads to a volcano plot [144] for elements in the hydrogen evolution reaction, see Figure 12a. Interestingly, when screening more effective catalytic species for the Mg-H_2 system, the experimental result does not always follow this prediction. Pozzo et al. [48,49] proposed an inverse volcano plot (see Figure 12b) combining the effects of hydrogen dissociation and hydrogen diffusion, suggesting that doping of Ni and Pd could provide the top catalytic activities. However, Ti and V have been experimentally demonstrated as strong catalysts, at least equivalent to Ni and Pd. In fact, the IV and V group elemental catalysts (such as Ti or V) in the hydrogen atmosphere may transform into hydride phases (TiH_x or VH_x) instead of their metallic phases. Therefore, a more comprehensive model and understanding of the catalytic behavior is still required to design an optimized catalyst.

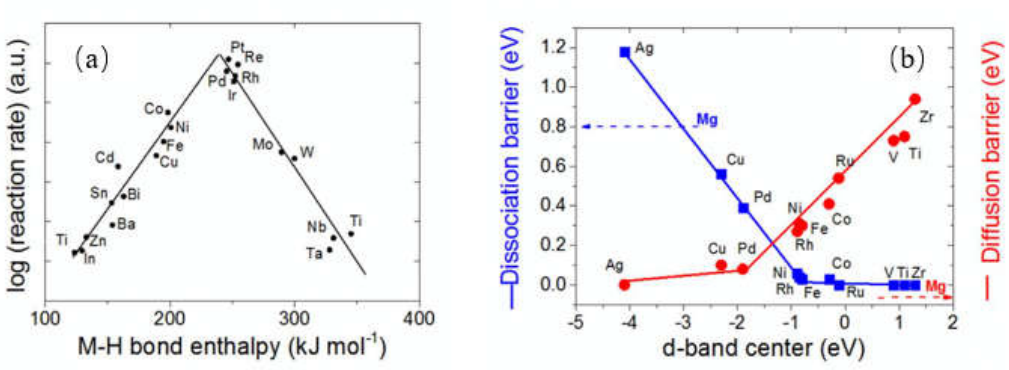

Figure 12. (**a**) Volcano plot for the hydrogen evolution reaction as function of the metal hydrogen bond enthalpy. (Reproduced with permission from ref. [144]. Copyright 1972 Elsevier). (**b**) Activation energy barrier for hydrogen dissociation (blue) and diffusion (red) of hydrogen on pure Mg and metal-doped Mg surfaces as a function of the d-band center positions. (Reproduced with permission from ref. [48]. Copyright 2009 Elsevier).

5.2. Surface Penetration

To improve dehydrogenation and hydrogenation kinetics, surface modification is necessary due to the presence of a surface oxide layer, which hinders the penetration of hydrogen atoms into the bulk. The continuous passive MgO/Mg(OH)$_2$ layer would easily cover the Mg/MgH$_2$ surface, even under inert gas with a trace amount of O$_2$/H$_2$O [145]. Recent work on the effect of air exposure on TiMn$_2$ catalyzed MgH$_2$, [146] showed that the direct air exposure leads to reduction of hydrogen storage capacity, but only moderate deterioration in kinetics. Further surface characterizations found that the surface of MgH$_2$ forms a layer with Mg(OH)$_2$ and MgO. However, the layer may crack during hydrogen cycling while the nanocomposite can be re-activated with the presence of catalyst. The doped catalyst particles on hydride surfaces can serve as paths to transfer hydrogen from surface to bulk, or from MgH$_2$ to the outside. This mechanism is often referred as the "hydrogen gateway" effect, as having been claimed in MgH$_2$-Nb [147] and MgH$_2$-Pt [148] catalyzed systems. In several in situ characterizations, intermediate phases (NbH$_{0.7}$ or TiH) were observed during dehydrogenation, supporting the assumption that the surface activated catalyst can create a hydrogen penetration path over the MgO layer.

5.3. Accelerating Hydrogen Diffusion

The addition of catalyst may play an important role in accelerating the hydrogen diffusion rate in the matrix. Due to the slow diffusion rate in MgH$_2$, it is thus believed that the reaction is likely to shift to diffusion-control when the forming hydride covers the particles during hydrogenation. For both hydrogenation and dehydrogenation processes, nano-doped catalytic species have been believed to help to accelerate hydrogen diffusion. This mechanism was often referred as the "hydrogen pathway" effect.

The "pathway effect" was first suggested by Friedrichs et al. [149] in the study of the MgH$_2$-Nb$_2$O$_5$ system. They suggested the hydrogen sorption improvement through a pathway effect of lower-oxidation-state Nb$_2$O$_{5-x}$, which was believed to help hydrogen transport into the particle. Ponthieu et al. [93] studied the structure and reversible deuterium uptake of MgD$_2$-TiD$_2$ nano-composites by X-ray and neutron diffractions, suggesting that TiD$_2$ addition limits the grain growth of Mg and MgD$_2$ phases and thus reduce the D-diffusion path. The study also found coherent coupling between TiD$_2$ and Mg/MgD$_2$ and the presence of sub-stoichiometric MgD$_{2-\eta}$ and TiD$_{2-\eta}$ phases, which are indications that the TiD$_2$ phase can favor the H-mobility. Note that the diffusion pathway may contribute to the grain boundaries between catalyst and matrix because the boundary and interface play the role of tunnels for fast hydrogen diffusion. Needless to say, nano-sized Mg/MgH$_2$ grains doped with catalysts lead to a significant number of boundaries, interfaces, and

dislocations. This mechanism is supported by many experimental works where a refined catalyzed Mg/MgH_2 composite is favored for the kinetics [150,151].

5.4. Nucleation and Growth

Nucleation and growth of the MgH_2 phase can be considered as the final step for the hydrogenation of Mg. The nucleation and growth of a hydride phase will lead to considerable interfacial energy changes due to the crystal structure difference between Mg metal and its forming hydride. Although, whether the rate-limiting step is controlled by nucleation and growth or hydrogen diffusion is still under debate; many investigations have successfully applied the Johnson–Mehl–Avrami–Kolmogorov (JMAK) model—a nucleation and growth model—to various catalyzed MgH_2 systems [152,153]. Some other results showed that the kinetics can be fitted by diffusion models, such as the Jander diffusion model [154,155]. In early works, Schimmel et al. [156] assumed that saturated catalyst particles in close contact with a Mg particle act as nucleation centers. A recent hydrogenography study of Mooij and Dam [157] showed evidence of nucleation and growth mechanism in the hydrogenation of the 1-dimensional nanoconfined Mg/TiH_2. They also suggested that the desorption mechanism is not simply the reverse of the absorption mechanism, and the energy barrier for nucleation of Mg is smaller than the nucleation of MgH_2. Danaie and Mitlin [158] established the metal hydride orientation relationship (OR) for the ball-milled MgH_2-TiF_3 system during hydrogen absorption and it was determined to be (110)MgH_2 || (−110−1)Mg and (111)MgH_2 || (01−11)Mg. The authors observed that during desorption the TiF_3 catalyst substantially increases the number of the newly formed Mg crystallites, which displays a strong texture correlation to the parent MgH_2 phase. Mulder et al. [159] made an assumption that MgF_2 may act as seeding crystals for MgH_2 because MgF_2 and MgH_2 have the same crystallographic structure and good lattice matching.

6. Kinetic Modeling

Kinetics study focuses on the quantitative interpretation of the reaction rates and of the factors upon which they depend. Early studies of the kinetics of the pure Mg-H_2 system attempted first-order reaction, second-order reaction, 2D contraction area, 3D diffusion, and Jander diffusion model. Due to the sluggish diffusion of hydrogen in the MgH_2 phase, it is believed that the hydrogenation of Mg is best described by the 3D diffusion-controlled contracting volume model [121]. As more doped systems have been examined, alternate kinetic models have been proposed to analyze the kinetic behavior of Mg-based hydrides [160]. Despite the debate and deviation, kinetic analysis has been recognized as a useful tool for Mg-based systems [161]. This section will summarize and discuss the kinetic models and analytic methods that are commonly applied for analyzing kinetics.

Basically, the reaction progress of a solid-gas system is defined as the fraction of the transformation, ξ ($0 \le \xi \le 1$), which is a function of reaction time t, and rate constant k, as shown in Equation (8):

$$\xi = f(k, t) \tag{8}$$

The rate constant k is defined as a specific rate and the rate coefficient and is a function of temperature. This rate constant k varies with temperature T following the Arrhenius Equation (9):

$$lnk = -\frac{E_a}{RT} + \ln A \tag{9}$$

In this relationship, activation energy can be calculated by the Arrhenius plot, which is lnk against the reciprocal of the absolute temperature $1/T$. As mentioned above, activation energy (E_a) for a catalyzed Mg/MgH_2 can be considered as a useful scale to evaluate the effectiveness of a catalyst. More importantly, the kinetic analysis could not only

calculate (E_a) and rate constant k, but also provide an understanding of reaction mechanisms. As can be seen in Table 5, the kinetic models can be divided into two categories: isothermal models, which are based on analysis of isothermal hydrogen absorption or desorption ($\xi - t$) curves; and non-isothermal models, which are based on ($\xi - t$) curves usually obtained under linearly increasing temperature (by utilizing TGA or Differential Scanning Calorimeters (DSC) techniques).

6.1. Isothermal Models

Several isothermal models, such as Johnson–Mehl–Avrami–Kolomogorov (JMAK) model [162], Jander model [163], Ginsling–Braunshtein (GB) model [164], contraction volume (CV) model [165], Valensi–Carter (V–C) model [166], and Chou model [163], have been applied to Mg-based systems. These models represent different rate-controlling processes, in other words, the JMAK model is established based on nucleation-growth-impingement mode; the Jander and GB models are derived from Fick's diffusion law and thus for a diffusion-controlled reaction; the CV model assumes that the hydrogen absorption/desorption is controlled by the interface (hydride/metal) movement. Generally, by examination of best-fitting using the above-mentioned and other models, rate-limiting step(s) and kinetic parameters (such as rate constant *k*, dimensionality *d*, Avrami exponent *n*), as well as corresponding physical interpretation, can be determined to investigate the hydrogenation/dehydrogenation behaviors. In addition, in some scenarios, the isothermal condition is difficult to maintain during hydrogenation, due to the highly exothermic reaction of Mg with H_2. Particular cautions are needed to minimize the thermal effect when dealing with catalyzed MgH_2 with fast hydrogenation rate and poor heat conductivity, which leads to heat accumulation of the material [71].

The classic JMAK model is widely accepted for studying the kinetics of various Mg-based materials [167]. The JMAK model assumes a solid-state phase transformation containing three overlapping procedures: nucleation, growth, and impingement. Theoretically, for the nucleation, it may be either saturation or linear continuous mode, and the former mode is usually described in heterogeneous catalysis. As for growth, both the interface-controlled growth and diffusion-controlled growth modes are taken into account within the JMAK model. Therefore, Avrami exponent *n* indicates different modes regarding the nucleation modes, dimensionality, and rate-controlling steps.

Li et al. [168] applied various kinetic models for ball-milled pure MgH_2, TiH_2-, $TiMn_2$- and VTiCr-catalyzed MgH_2 under different temperatures and pressures, showing the best-fitting model for hydrogenation of the various materials is the JMAK model. However, problems with the JMAK model still exist. It was pointed out that the obtained values of Avrami exponent *n* are in a very wide range (n = 0.11–1.64), which is difficult to interpret using the classic JMAK theory. Small values of *n* have also been reported in the hydrogenation of Mg-Ti [168] and Mg-V-Nb [130] thin films. Overall, the kinetic parameters and corresponding discussions obtained from isothermal modeling are usually difficult to be conclusive. As pointed out in the review by Pang and Li [161], it is difficult to elucidate the assumption and derivation steps of the kinetics models, and it is also difficult to select proper methods to analyze the experimental data.

Table 5. Kinetic models applied for hydrogenation. (Reproduced with permission from ref. [71]. Copyright 2014 Elsevier)

Model	Kinetic equation
Johnson-Mehl-Avrami (JMA)	$\ln(-\ln(1-\xi)) = \ln(k) + n\ln(t)$
Jander diffusion model (JMD)	$(1-(1-\xi)^{1/3})^2 = kt$
1-D diffusion	$\xi^2 = kt$
2-D diffusion (Bidimensional partical shape)	$(1-\xi)\ln(1-\xi) + \xi = kt$
3-D diffusion (Ginsling-Braunshteinn model)	$(1-2\xi/3) - (1-\xi)^{2/3} = kt$
2-D contracting area	$1-(1-\xi)^{1/2} = kt$
3-D contracting volume	$1-(1-\xi)^{1/3} = kt$

6.2. Non-Isothermal Method

The dehydrogenation kinetics method is based on Kissinger's theory. It allows deriving activation energy by measuring the weight change via TGA, or heat flow via DSC under a constant heating rate.

$$\ln\left(\frac{\beta}{T_{max}^2}\right) = -\frac{E_a}{R}\left(\frac{1}{T_{max}}\right) + F_{KAS}(\xi) \quad (10)$$

In Equation (10), T_{max} is the temperature when the reaction rate reaches the maximum, β is the heating rate, E_a is the activation energy, R is the gas constant, and $F_{KAS}(\xi)$ is the function of the fraction of transformation ξ. The Kissinger method has been widely employed for the calculation of dehydrogenation E_a of catalyzed MgH_2 materials. This method has the advantages of efficiency and convenience to evaluate dehydrogenation activation energy. However, the estimation for kinetics cannot be conducted under different hydrogen pressures, since most of the TGA/DSC tests are performed under the flow of inert gas. Consequently, it is difficult to identify the actual process that is controlling the reaction rates, which leads to inconsistent interpretations that cannot be reliability validated.

6.3. Activation Energies

The activation energies (summarized in Table 4) for various Ti-additive doped MgH_2 systems are plotted in Figure 13. For the reactions of pure MgH_2, the activation energies are reported to be 160 kJ/mol for dehydrogenation and 100 kJ/mol for hydrogenation [138]. Doping with different Ti-based catalysts reduced the MgH_2 dehydrogenation E_a to as low as approximately 70 kJ/mol. The majority of dehydrogenation E_a values were derived using TGA/DSC and the Kissinger method. It is interesting to find that many catalyzed systems reported dehydrogenation E_a in the range of 70–75 kJ/mol, which corresponds with the ΔH of MgH_2 (74.5 kJ/mol·H_2) although there are some outliers in the reported values. Note that in general the calculated dehydrogenation E_a should be no less than the ΔH (see Figure 5). The low values of E_a imply that in these systems the energy barriers of dehydrogenation have been largely overcome. Additionally, some abnormally low E_a should be carefully examined in terms of the systematic deviations or apparatus errors during the experiments. For hydrogenation, many published hydrogenation E_a are below 30 kJ/mol, which is significantly lower than that of pure MgH_2 [70, 71]. From the survey of published E_a data, it is shown that the kinetics can be significantly enhanced by Ti-based addition. Ti and Ti hydrides, halides, and intermetallic compounds present excellent catalytic effects.

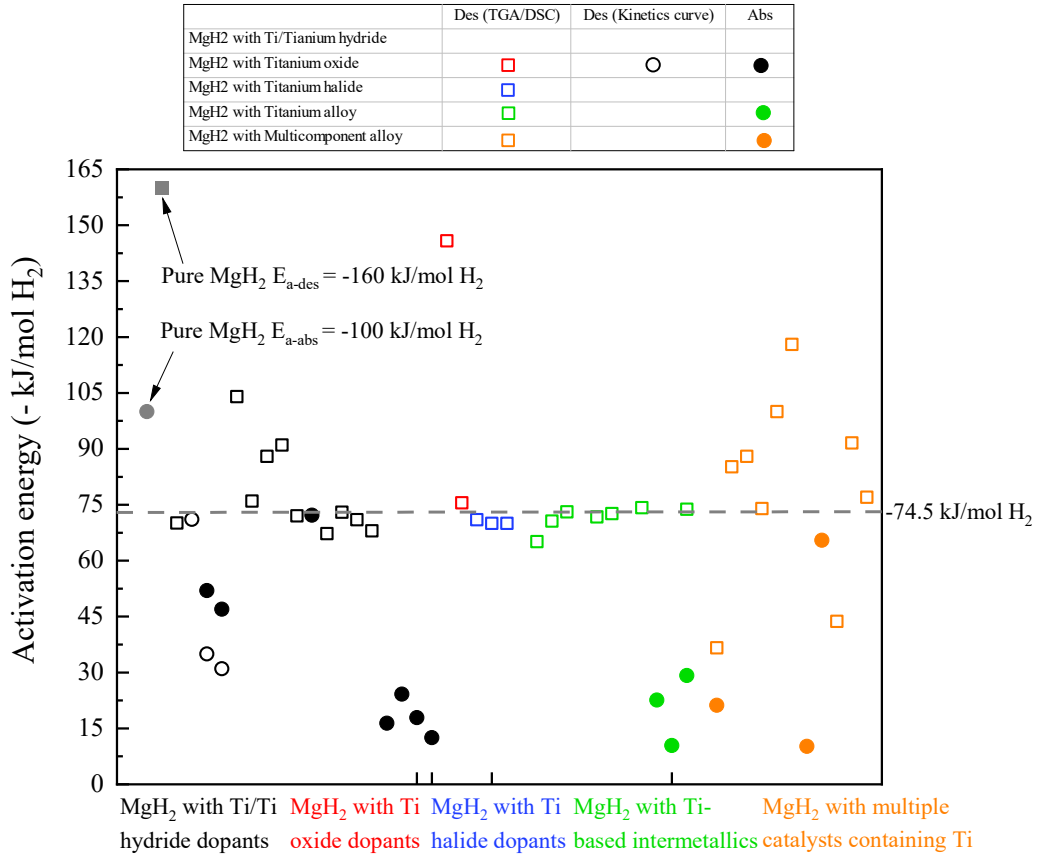

Figure 13. Apparent activation energies derived from experiments of kinetic rates for the hydrogenation and dehydrogenation in MgH_2 with the addition of various Ti-based catalysts.

7. Summary and Perspectives

Mg-based hydrides have shown great prospects as high-energy-density media for hydrogen storage and thermal energy storage. The high hydrogen capacity, abundant resources, reversibility, and low toxicity make Mg-based materials promising candidates. It has been well recognized that doping Ti-based additive is an effective method to enhance the hydrogen storage properties of MgH_2. The catalytic doping combined with ball-milling techniques is widely used for synthesizing nano-structured MgH_2-additive composite. Additionally, other synthetic methods such as thin film deposition and chemical methods have been employed. Recent research showed that Mg-based material can be modified into various nano-structures, while the kinetics are dramatically improved by catalytic doping. Various types of Ti-based catalysts including hydrides, oxides, halides, and intermetallics showed positive effects in improving dehydrogenation and hydrogenation kinetics. However, it is still difficult to assess the effectiveness of different catalysts.

The survey of reported activation energies shows that the energy barrier can be largely overcome by the use of Ti-based additives. The mechanism of catalysis can be resolved into several steps, for example, for hydrogenation: hydrogen dissociation, surface penetration, diffusion, hydride nucleation, and growth. Although a comprehensive understanding of the role of Ti-based catalysts still remains unclear, there has been evidenced that catalysts do play important roles in promoting some of the steps. It was believed that the doped catalyst species can reduce the dissociation energy barrier of the hydrogen molecule, and can also facilitate the hydrogen diffusion in the Mg/MgH_2 matrix. Kinetic modeling could become a more useful tool for interpreting the controlling steps of the reactions. Future mechanism works should be directed to observe catalytic activities

and microstructure evolution during highly controlled reaction conditions to provide closer comparisons with boundary conditions for the alternative models used for interpretations.

Author Contributions: C.Z. conceived and designed the concept. C.Z. and J.Z. collected the references and contributed to the writing of the original draft. R.C.B.J. design some of the main ideas for the construction of the paper. C.Z. contribute to the supervision and funding acquisition. C.Z., R.C.B.J. and Z.Z.F. contribute to the review and editing of the review. All authors have read and agreed to the published version of the manuscript.

Funding: National Natural Science Funds for Young Scientists of China (Grant No.51704336); Innovation-Driven Project of Central South University (Grant No. 2020CX025).

Acknowledgments: C.Z. acknowledges the National Natural Science Funds for Young Scientists of China (Grant No.51704336) and the Innovation-Driven Project of Central South University (Grant No. 2020CX025). J.Z. thanks the China Scholarship Council (CSC) for financial support.

Conflicts of Interest: The authors declare no conflict of interest.

References

1. Harapan, H.; Mudatsir, M.; Yufika, A.; Nawawi, Y.; Wahyuniati, N.; Anwar, S.; Yusri, F.; Haryanti, N.; Wijayanti, N.P.; Rizal, R.; et al. Hydrogen and fuel cells: Towards a sustainable energy future. *Energy Policy* **2008**, *36*, 4356–4362.
2. Felderhoff, M.; Weidenthaler, C.; von Helmolt, R.; Eberle, U. Hydrogen storage: The remaining scientific and technological challenges. *Phys Chem Chem Phys* **2007**, *9*, 2643–2653.
3. Jollibois MP. Sur la formule du derive organo-magnesien et sur l'hydrure de magnesium. *Compt. Rend.* **1912**, *155*, 353–355.
4. Dymova, T.N.; Sterlyadkina, Z.K.; Safronov, V.G. On the preparation of magnesium hydride. *Russ. J. Inorg. Chem.* **1961**, *6*, 763–767.
5. Schlapbach, L.; Züttel, A. Hydrogen-storage materials for mobile applications. *Nature* **2001**, *414*, 353–358.
6. Fang, Z.Z.; Zhou, C.; Fan, P.; Udell, K.S.; Bowman, R.C.; Vajo, J.J.; Purewal, J.J.; Kekelia, B. Metal hydrides based high energy density thermal battery. *J. Alloy. Compd.* **2015**, *645*, S184–S189.
7. Li, J.; Li, B.; Shao, H.; Li, W.; Lin, H. Catalysis and downsizing in Mg-based hydrogen storage materials. *Catalysts* **2018**, *8*, 89.
8. Sadhasivam, T.; Kim, H.-T.; Jung, S.; Roh, S.-H.; Park, J.-H.; Jung, H.-Y. Dimensional effects of nanostructured Mg/MgH 2 for hydrogen storage applications: A review. *Renew. Sustain. Energy Rev.* **2017**, *72*, 523–534.
9. Cheng, F.; Tao, Z.; Liang, J.; Chen, J. Efficient hydrogen storage with the combination of lightweight Mg/MgH2 and nanostructures. *Chem. Commun.* **2012**, *48*, 7334–7343.
10. Zhang, X.; Liu, Y.; Hu, J.; Gao, M.; Pan, H. Empowering hydrogen storage performance of MgH2 by nanoengineering and nanocatalysis. *Mater. Today Nano* **2020**, *9*, 100064.
11. Aguey-Zinsou, K.-F.; Ares-Fernández, J.-R. Hydrogen in magnesium: New perspectives toward functional stores. *Energy Environ. Sci.* **2010**, *3*, 526–543.
12. de Jongh, P.E.; Adelhelm, P. Nanosizing and nanoconfinement: New strategies towards meeting hydrogen storage goals. *ChemSusChem* **2010**, *3*, 1332–1348.
13. Shao, H.; He, L.; Lin, H.; Li, H.-W. Progress and Trends in Magnesium-Based Materials for Energy-Storage Research: A Review. *Energy Technol.* **2018**, *6*, 445–458.
14. Webb, C.A. A review of catalyst-enhanced magnesium hydride as a hydrogen storage material. *J. Phys. Chem. Solids* **2015**, *84*, 96–106.
15. Yartys, V.; Lototskyy, M.; Akiba, E.; Albert, R.; Antonov, V.; Ares, J.; Baricco, M.; Bourgeois, N.; Buckley, C.; Von Colbe, J.B.; et al. Magnesium based materials for hydrogen based energy storage: Past, present and future. *Int. J. Hydrogen Energy* **2019**, *44*, 7809–7859.
16. Luo, Q.; Li, J.; Li, B.; Liu, B.; Shao, H.; Li, Q. Kinetics in Mg-based hydrogen storage materials: Enhancement and mechanism. *J. Magnes. Alloy.* **2019**, *7*, 58–71.
17. Xie, X.; Chen, M.; Hu, M.; Wang, B.; Yu, R.; Liu, T. Recent advances in magnesium-based hydrogen storage materials with multiple catalysts. *Int. J. Hydrog. Energy* **2019**, *44*, 10694–10712.
18. Zhang, Q.; Zang, L.; Huang, Y.; Gao, P.; Jiao, L.; Yuan, H.; Wang, Y. Improved hydrogen storage properties of MgH2 with Ni-based compounds. *Int. J. Hydrog. Energy* **2017**, *42*, 24247–24255.
19. Zhang, J.; Li, Z.; Wu, Y.; Guo, X.; Ye, J.; Yuan, B.; Wang, S.; Jiang, L. Recent advances on the thermal destabilization of Mg-based hydrogen storage materials. *RSC Adv.* **2019**, *9*, 408–428.
20. Stampfer, J.F.; Holley, C.E.; Suttle, J.F. The magnesium-hydrogen system1-3. *J. Am. Chem. Soc.* **1960**, *82*, 3504–3508.
21. Jain, I.; Lal, C.; Jain, A. Hydrogen storage in Mg: A most promising material. *Int. J. Hydrog. Energy* **2010**, *35*, 5133–5144.
22. Vajeeston, P.; Ravindran, P.; Hauback, B.C.; Fjellvåg, H.; Kjekshus, A.; Furuseth, S.; Hanfland, M. Structural stability and pressure-induced phase transitions in MgH2. *Phys. Rev. B* **2006**, *73*, 224102-224102.

23. Dornheim, M.; Doppiu, S.; Barkhordarian, G.; Boesenberg, U.; Klassen, T.; Gutfleisch, O.; Bormann, R. Hydrogen storage in magnesium-based hydrides and hydride composites. *Scr. Mater.* **2007**, *56*, 841–846.
24. Vajeeston, P.; Ravindran, P.; Kjekshus, A.; Fjellvag, H. Pressure-induced structural transitions in MgH2. *Phys. Rev. Lett.* **2002**, *89*, 175506.
25. Varin, R.A.; Czujko, T.; Wronski, Z. Particle size, grain size and γ-MgH2effects on the desorption properties of nanocrystalline commercial magnesium hydride processed by controlled mechanical milling. *Nanotechnology* **2006**, *17*, 3856–3865.
26. Felderhoff, M.; Bogdanović, B. High temperature metal hydrides as heat storage materials for solar and related applications. *Int. J. Mol. Sci.* **2009**, *10*, 325–344.
27. Satyapal, S.; Petrovic, J.; Read, C.; Thomas, G.; Ordaz, G. The U.S. Department of Energy's National Hydrogen Storage Project: Progress towards meeting hydrogen-powered vehicle requirements. *Catal. Today* **2007**, *120*, 246–256.
28. Kohno, T.; Tsuruta, S.; Kanda, M. The hydrogen storage properties of new Mg2Ni alloy. *J. Electrochem. Soc.* **1996**, *143*, 198–199.
29. Shao, H.; Wang, Y.; Xu, H.; Li, X. Preparation and hydrogen storage properties of nanostructured Mg2Cu alloy. *J. Solid State Chem.* **2005**, *178*, 2211–2217.
30. Bououdina, M.; Guo, Z.X. Comparative study of mechanical alloying of (Mg+ Al) and (Mg+ Al+ Ni) mixtures for hydrogen storage. *J. Alloy. Compd.* **2002**, *336*, 222–231.
31. Bruzzone, G.; Costa, G.; Ferretti, M.; Olcese, G. Hydrogen storage in Mg51Zn20. *Int. J. Hydrog. Energy* **1983**, *8*, 459–461.
32. Chaudhary, A.-L.; Sheppard, D.A.; Paskevicius, M.; Webb, C.J.; Gray, E.M.; Buckley, C.E. Mg2Si Nanoparticle Synthesis for High Pressure Hydrogenation. *J. Phys. Chem. C* **2014**, *118*, 1240–1247.
33. Zhou, C.; Fang, Z.Z.; Lu, J.; Zhang, X. Thermodynamic and kinetic destabilization of magnesium hydride using Mg-In solid solution alloys. *J. Am. Chem. Soc.* **2013**, *135*, 10982–10985.
34. Si, T.; Cao, Y.; Zhang, Q.; Sun, D.; Ouyang, L.; Zhu, M. Enhanced hydrogen storage properties of a Mg–Ag alloy with solid dissolution of indium: A comparative study. *J. Mater. Chem. A* **2015**, *3*, 8581–8589.
35. Spassov, T.; Lyubenova, L.; Köster, U.; Baró, M.D. Mg–Ni–RE nanocrystalline alloys for hydrogen storage. *Mater. Sci. Eng. A* **2004**, *375–377*, 794–799.
36. Asano, K.; Enoki, H.; Akiba, E. Effect of Li Addition on Synthesis of Mg-Ti BCC Alloys by means of Ball Milling. *Mater. Trans.* **2007**, *48*, 121–126.
37. Asano, K.; Akiba, E. Direct synthesis of Mg–Ti–H FCC hydrides from MgH2 and Ti by means of ball milling. *J. Alloy. Compd.* **2009**, *481*, L8–L11.
38. Asano, K.; Enoki, H.; Akiba, E. Synthesis of HCP, FCC and BCC structure alloys in the Mg–Ti binary system by means of ball milling. *J. Alloy. Compd.* **2009**, *480*, 558–563.
39. Asano, K.; Enoki, H.; Akiba, E. Synthesis process of Mg–Ti BCC alloys by means of ball milling. *J. Alloy. Compd.* **2009**, *486*, 115–123.
40. Vermeulen, P.; van Thiel, E.F.; Notten, P.H. Ternary MgTiX-alloys: A promising route towards low-temperature, high-capacity, hydrogen-storage materials. *Chemistry* **2007**, *13*, 9892–9898.
41. Jain, A.; Miyaoka, H.; Ichikawa, T. Destabilization of lithium hydride by the substitution of group 14 elements: A review. *Int. J. Hydrog. Energy* **2016**, *41*, 5969–5978.
42. Wagemans, R.W.P.; van Lenthe, J.H.; de Jongh, P.E.; van Dillen, A.J.; de Jong, K.P. Hydrogen storage in magnesium clusters: Quantum chemical study. *J. Am. Chem. Soc.* **2005**, *127*, 16675–16680.
43. Zhang, J.; Yan, S.; Qu, H. Stress/strain effects on thermodynamic properties of magnesium hydride: A brief review. *Int. J. Hydrog. Energy* **2017**, *42*, 16603–16610.
44. Berube, V.; Chen, G.; Dresselhaus, M. Impact of nanostructuring on the enthalpy of formation of metal hydrides. *Int. J. Hydrog. Energy* **2008**, *33*, 4122–4131.
45. Zhu, M.; Lu, Y.; Ouyang, L.; Wang, H. Thermodynamic Tuning of Mg-Based Hydrogen Storage Alloys: A Review. *Materials* **2013**, *6*, 4654–4674.
46. Bououdina, M.; Grant, D.; Walker, G. Review on hydrogen absorbing materials—structure, microstructure, and thermodynamic properties. *Int. J. Hydrog. Energy* **2006**, *31*, 177–182.
47. Sun, Y.; Shen, C.; Lai, Q.; Liu, W.; Wang, D.-W.; Aguey-Zinsou, K.-F. Tailoring magnesium based materials for hydrogen storage through synthesis: Current state of the art. *Energy Storage Mater.* **2018**, *10*, 168–198.
48. Pozzo, M.; Alfè, D. Hydrogen dissociation and diffusion on transition metal (=Ti, Zr, V, Fe, Ru, Co, Rh, Ni, Pd, Cu, Ag)-doped Mg, 0001, surfaces. *Int. J. Hydrog. Energy* **2009**, *34*, 1922–1930.
49. Pozzo, M.; Alfe, D.; Amieiro, A.; French, S.; Pratt, A. Hydrogen dissociation and diffusion on Ni- and Ti-doped Mg, 0001, surfaces. *J. Chem. Phys.* **2008**, *128*, 094703.
50. Spatz, P.; Aebischer, H.A.; Krozer, A.; Schlapbach, L. The Diffusion of H in Mg and the Nucleation and Growth of MgH2in Thin Films*. *Z. Phys. Chem.* **1993**, *181*, 393–397.
51. Zhou, C. A Study of Advanced Magnesium-Based Hydride and Development of a Metal Hydride Thermal Battery System. Ph.D. Thesis, The University of Utah, Salt Lake City, UT, USA, 2015.
52. Jain, A.; Agarwal, S.; Ichikawa, T. Catalytic tuning of sorption kinetics of lightweight hydrides: A review of the materials and mechanism. *Catalysts* **2018**, *8*, 651.
53. Liang, G.; Huot, J.; Boily, S.; Neste, A.V.; Schulz, R. Catalytic effect of transition metals on hydrogen sorption in nanocrystalline ball milled MgH–Tm (Tm = Ti, V, Mn, Fe and Ni). *J. Alloy. Compd.* **1999**, *292*, 247–252.

54. Rizo-Acosta, P.; Cuevas, F.; Latroche, M. Hydrides of early transition metals as catalysts and grain growth inhibitors for enhanced reversible hydrogen storage in nanostructured magnesium. *J. Mater. Chem. A* **2019**, *7*, 23064–23075.
55. Pasquini, L.; Callini, E.; Brighi, M.; Boscherini, F.; Montone, A.; Jensen, T.R.; Maurizio, C.; Antisari, M.V.; Bonetti, E. Magnesium nanoparticles with transition metal decoration for hydrogen storage. *J. Nanopart. Res.* **2011**, *13*, 5727–5737.
56. Vincent, S.; Lang, J.; Huot, J. Addition of catalysts to magnesium hydride by means of cold rolling. *J. Alloy. Compd.* **2012**, *512*, 290–295.
57. Ma, L.-P.; Wang, P.; Kang, X.-D.; Cheng, H.-M. Preliminary investigation on the catalytic mechanism of TiF3 additive in MgH2–TiF3 H-storage system. *J. Mater. Res.* **2011**, *22*, 1779–1786.
58. Zhou, C.; Fang, Z.Z.; Ren, C.; Li, J.; Lu, J. Effect of Ti Intermetallic catalysts on hydrogen storage properties of magnesium hydride. *J. Phys. Chem. C* **2013**, *117*, 12973–12980.
59. Choi, Y.J.; Choi, J.W.; Sohn, H.Y.; Ryu, T.; Hwang, K.S.; Fang, Z.Z. Chemical vapor synthesis of Mg–Ti nanopowder mixture as a hydrogen storage material. *Int. J. Hydrog. Energy* **2009**, *34*, 7700–7706.
60. Patelli, N.; Migliori, A.; Pasquini, L. Reversible metal-hydride transformation in Mg-Ti-H nanoparticles at remarkably low temperatures. *ChemPhysChem* **2019**, *20*, 1325–1333.
61. Choi, E.; Song, M.Y. Hydriding and dehydriding features of a titanium-added magnesium hydride composite, materials. *Science* **2020**, *26*, 199–204.
62. Lotoskyy, M.; Denys, R.; Yartys, V.A.; Eriksen, J.; Goh, J.; Nyamsi, S.N.; Sita, C.; Cummings, F. An outstanding effect of graphite in nano-MgH2-TiH2 on hydrogen storage performance dagger. *J. Mater. Chem. A* **2018**, *6*, 10740–10754.
63. Croston, D.; Grant, D.; Walker, G. The catalytic effect of titanium oxide based additives on the dehydrogenation and hydrogenation of milled MgH2. *J. Alloy. Compd.* **2010**, *492*, 251–258.
64. Cui, J.; Wang, H.; Liu, J.; Ouyang, L.; Zhang, Q.; Sun, D.; Yao, X.; Zhu, M. Remarkable enhancement in dehydrogenation of MgH2 by a nano-coating of multi-valence Ti-based catalysts. *J. Mater. Chem. A* **2013**, *492*, 251–258.
65. Calizzi, M.; Venturi, F.; Ponthieu, M.; Cuevas, F.; Morandi, V.; Perkisas, T.; Bals, S.; Pasquini, L. Gas-phase synthesis of Mg–Ti nanoparticles for solid-state hydrogen storage. *Phys. Chem. Chem. Phys.* **2016**, *18*, 141–148.
66. Lu, C.; Zou, J.; Shi, X.; Zeng, X.; Ding, W. Synthesis and hydrogen storage properties of core–shell structured binary Mg@ Ti and ternary Mg@ Ti@ Ni composites. *Int. J. Hydrog. Energy* **2017**, *42*, 2239–2247.
67. Choi, Y.J.; Lu, J.; Sohn, H.Y.; Fang, Z.Z.; Rönnebro, E. Effect of milling parameters on the dehydrogenation properties of the Mg–Ti–H system. *J. Phys. Chem. C* **2009**, *113*, 19344–19350.
68. Choi, Y.J.; Lu, J.; Sohn, H.Y.; Fang, Z.Z. Hydrogen storage properties of the Mg–Ti–H system prepared by high-energy–high-pressure reactive milling. *J. Power Sources* **2008**, *180*, 491–497.
69. Lu, J.; Choi, Y.J.; Fang, Z.Z.; Sohn, H.Y.; Rönnebro, E. Hydrogenation of Nanocrystalline Mg at Room Temperature in the Presence of TiH2. *J. Am. Chem. Soc.* **2010**, *132*, 6616–6617.
70. Li, J.; Zhou, C.; Fang, Z.Z.; Bowman, R.C., Jr.; Lu, J.; Ren, C. Isothermal hydrogenation kinetics of ball-milled nano-catalyzed magnesium hydride. *Materialia* **2019**, *5*, 100227.
71. Li, J.; Fan, P.; Fang, Z.Z.; Zhou, C. Kinetics of isothermal hydrogenation of magnesium with TiH2 additive. *Int. J. Hydrog. Energy* **2014**, *39*, 7373–7381.
72. Liu, T.; Chen, C.; Wang, F.; Li, X. Enhanced hydrogen storage properties of magnesium by the synergic catalytic effect of TiH1.971 and TiH1.5 nanoparticles at room temperature. *J. Power Sources* **2014**, *267*, 69–77.
73. Manivasagam, T.G.; Magusin, P.C.M.M.; Iliksu, M.; Notten, P.H.L. Influence of Nickel and Silicon Addition on the Deuterium Siting and Mobility in fcc Mg–Ti Hydride Studied with2H MAS NMR. *J. Phys. Chem. C* **2014**, *118*, 10606–10615.
74. Oelerich, W.; Klassen, T.; Bormann, R. Mg-based hydrogen storage materials with improved hydrogen sorption. *Mater. Trans.* **2001**, *42*, 1588–1592.
75. Wang, P.; Wang, A.; Zhang, H.; Ding, B.; Hu, Z. Hydrogenation characteristics of Mg–TiO (rutile) composite. *J. Alloy. Compd.* **2000**, *313*, 218–223.
76. Chen, M.; Xiao, X.; Zhang, M.; Liu, M.; Huang, X.; Zheng, J.; Zhang, Y.; Jiang, L.; Chen, L. Excellent synergistic catalytic mechanism of in-situ formed nanosized Mg2Ni and multiple valence titanium for improved hydrogen desorption properties of magnesium hydride. *Int. J. Hydrog. Energy* **2019**, *44*, 1750–1759.
77. Jangir, M.; Gattia, D.M.; Peter, A.; Jain, I.P. *Effect of Ti-Additives on Hydrogenation/Dehydrogenation Properties of MgH2 Proceedings of the 15th International Conference on Concentrator Photovoltaic Systems (CPV-15), Fes, Marocco, 25–27 March 2019*; AIP Publishing: College Park, MD, USA, 2019; Volume 2145, p. 020006.
78. Jain, A.; Agarwal, S.; Kumar, S.; Yamaguchi, S.; Miyaoka, H.; Kojima, Y.; Ichikawa, T. How does TiF4 affect the decomposition of MgH2 and its complex variants?—An XPS investigation. *J. Mater. Chem. A* **2017**, *5*, 15543–15551.
79. Jangir, M.; Jain, A.; Yamaguchi, S.; Ichikawa, T.; Lal, C.; Jain, I. Catalytic effect of TiF4 in improving hydrogen storage properties of MgH2. *Int. J. Hydrog. Energy* **2016**, *41*, 14178–14183.
80. Malka, I.; Czujko, T.; Bystrzycki, J. Catalytic effect of halide additives ball milled with magnesium hydride. *Int. J. Hydrog. Energy* **2010**, *35*, 1706–1712.
81. Kalisvaart, W.; Harrower, C.; Haagsma, J.; Zahiri, B.; Luber, E.; Ophus, C.; Poirier, E.; Fritzsche, H.; Mitlin, D. Hydrogen storage in binary and ternary Mg-based alloys: A comprehensive experimental study. *Int. J. Hydrog. Energy* **2010**, *35*, 2091–2103.
82. Zahiri, B.; Amirkhiz, B.S.; Mitlin, D. Hydrogen storage cycling of MgH2 thin film nanocomposites catalyzed by bimetallic Cr Ti. *Appl. Phys. Lett.* **2010**, *97*, 083106.

83. Yao, X.; Wu, C.; Du, A.; Zou, J.; Zhu, Z.; Wang, P.; Cheng, H.; Smith, S.C.; Lu, G. Metallic and carbon nanotube-catalyzed coupling of hydrogenation in magnesium. *J. Am. Chem. Soc.* **2007**, *129*, 15650–15654.
84. Liu, T.; Chen, C.; Wang, H.; Wu, Y. Enhanced hydrogen storage properties of Mg–Ti–V nanocomposite at moderate temperatures. *J. Phys. Chem. C* **2014**, *118*, 22419–22425.
85. Berlouis, L.E.A.; Honnor, P.; Hall, P.J.; Morris, S.; Dodd, S.B. An investigation of the effect of Ti, Pd and Zr on the dehydriding kinetics of MgH2. *J. Mater. Sci.* **2006**, *41*, 6403–6408.
86. Chen, C.; Wang, J.; Wang, H.; Liu, T.; Xu, L.; Li, X.I. Improved kinetics of nanoparticle-decorated Mg-Ti-Zr nanocomposite for hydrogen storage at moderate temperatures. *Mater. Chem. Phys.* **2018**, *206*, 21–28.
87. Huang, X.; Xiao, X.; Wang, X.; Wang, C.; Fan, X.; Tang, Z.; Wang, C.; Wang, Q.; Chen, L. Synergistic catalytic activity of porous rod-like TMTiO3 (TM = Ni and Co) for reversible hydrogen storage of magnesium hydride. *J. Phys. Chem. C* **2018**, *122*, 27973–27982.
88. Daryani, M.; Simchi, A.; Sadati, M.; Hosseini, H.M.; Targholizadeh, H.; Khakbiz, M. Effects of Ti-based catalysts on hydrogen desorption kinetics of nanostructured magnesium hydride. *Int. J. Hydrog. Energy* **2014**, *39*, 21007–21014.
89. Chen, M.; Xiao, X.; Zhang, M.; Zheng, J.; Liu, M.; Wang, X.; Jiang, L.; Chen, L. Highly dispersed metal nanoparticles on TiO2 acted as nano redox reactor and its synergistic catalysis on the hydrogen storage properties of magnesium hydride. *Int. J. Hydrog. Energy* **2019**, *44*, 15100–15109.
90. Zhou, C.; Fang, Z.Z.; Sun, P. An experimental survey of additives for improving dehydrogenation properties of magnesium hydride. *J. Power Sources* **2015**, *278*, 38–42.
91. Cui, J.; Liu, J.; Wang, H.; Ouyang, L.; Sun, D.; Zhu, M.; Yao, X. Mg–TM (TM: Ti, Nb, V, Co, Mo or Ni) core–shell like nanostructures: Synthesis, hydrogen storage performance and catalytic mechanism. *J. Mater. Chem. A* **2014**, *2*, 9645-9655.
92. Lu, J.; Choi, Y.J.; Fang, Z.Z.; Sohn, H.Y.; Rönnebro, E. Hydrogen storage properties of nanosized MgH2-0.1TiH2 prepared by ultrahigh-energy-high-pressure milling. *J. Am. Chem. Soc.* **2009**, *131*, 15843–15852.
93. Ponthieu, M.; Cuevas, F.; Fernández, J.F.; Laversenne, L.; Porcher, F.; Latroche, M. Structural properties and reversible deuterium loading of MgD2–TiD2 nanocomposites. *J. Phys. Chem. C* **2013**, *117*, 18851–18862.
94. Emery, S.B.; Sorte, E.G.; Bowman, R.C.; Fang, Z.Z.; Ren, C.; Majzoub, E.H.; Conradi, M.S. Detection of fluorite-structured MgD2/TiD2: Deuterium NMR. *J. Phys. Chem.* **2015**, *119*, 7656–7661.
95. Kyoi, D.; Sato, T.; Rönnebro, E.; Kitamura, N.; Ueda, A.; Ito, M.; Katsuyama, S.; Hara, S.; Noréus, D.; Sakai, T. A new ternary magnesium–titanium hydride Mg7TiHx with hydrogen desorption properties better than both binary magnesium and titanium hydrides. *J. Alloy. Compd.* **2004**, *372*, 213–217.
96. Oelerich, W.; Klassen, T.; Bormann, R. Metal oxides as catalysts for improved hydrogen sorption in nanocrystalline Mg-based materials. *J. Alloy. Compd.* **2001**, *315*, 237–242.
97. Pukazhselvan, D.; Nasani, N.; Correia, P.; Carbó-Argibay, E.; Otero-Irurueta, G.; Stroppa, D.G.; Fagg, D.P. Evolution of reduced Ti containing phase(s) in MgH2/TiO2 system and its effect on the hydrogen storage behavior of MgH2. *J. Power Sources* **2017**, *362*, 174–183.
98. Zhang, M.; Xiao, X.; Luo, B.; Liu, M.; Chen, M.; Chen, L. Superior de/hydrogenation performances of MgH2 catalyzed by 3D flower-like TiO2@C nanostructures. *J. Energy Chem.* **2020**, *46*, 191–198.
99. Berezovets, V.; Denys, R.; Zavaliy, I.; Kosarchyn, Y. Effect of Ti-based nanosized additives on the hydrogen storage properties of MgH2. *Int. J. Hydrog. Energy* **2021**, doi:10.1016/j.ijhydene.2021.03.019.
100. Jin, S.-A.; Shim, J.-H.; Cho, Y.W.; Yi, K.-W. Dehydrogenation and hydrogenation characteristics of MgH2 with transition metal fluorides. *J. Power Sources* **2007**, *172*, 859–862.
101. Wang, Y.; Zhang, Q.; Wang, Y.; Jiao, L.; Yuan, H. Catalytic effects of different Ti-based materials on dehydrogenation performances of MgH 2. *J. Alloy. Compd.* **2015**, *645*, S509–S512.
102. Guoxian, L.; Erde, W.; Shoushi, F. Hydrogen absorption and desorption characteristics of mechanically milled Mg-35 wt%$FeTi_{1.2}$ powders. *J. Alloy. Compd.* **1995**, *223*, 111–114.
103. Reule, H.; Hirscher, M.; Weißhardt, A.; Kronmüller, H. Hydrogen desorption properties of mechanically alloyed MgH2 composite materials. *J. Alloy. Compd.* **2000**, *305*, 246–252.
104. Cui, N.; Luan, B.; Zhao, H.; Liu, H.K.; Dou, S.X. Synthesis and electrode characteristics of the new composite alloys Mg2Ni-xwt%Ti2Ni. *J. Alloy. Compd.* **1996**, *240*, 229–234.
105. Hu, Y.; Zhang, H.; Wang, A.; Ding, B.; Hu, Z. Preparation and hydriding/dehydriding properties of mechanically milled Mg–30 wt% TiMn1.5 composite. *J. Alloy. Compd.* **2003**, *354*, 296–302.
106. El-Eskandarany, M.S.; Shaban, E.; Aldakheel, F.; Alkandary, A.; Behbehani, M.; Al-Saidi, M. Synthetic nanocomposite MgH2/5 wt. % TiMn2 powders for solid-hydrogen storage tank integrated with PEM fuel cell. *Sci. Rep.* **2017**, *7*, 13296.
107. El-Eskandarany, M.S.; Al-Ajmi, F.; Banyan, M.; Al-Duweesh, A. Synergetic effect of reactive ball milling and cold pressing on enhancing the hydrogen storage behavior of nanocomposite MgH2/10 wt% TiMn2 binary system. *Int. J. Hydrog. Energy* **2019**, *44*, 26428–26443.
108. Dai, J.H.; Jiang, X.W.; Song, Y. Stability and hydrogen adsorption properties of Mg/TiMn2 interface by first principles calculation. *Surf. Sci.* **2016**, *653*, 22–26.
109. Hanada, N.; Ichikawa, T.; Fujii, H. Catalytic effect of Ni nano-particle and Nb oxide on H-desorption properties in MgH2 prepared by ball milling. *J. Alloy. Compd.* **2005**, *404–406*, 716–719.

110. Pourabdoli, M.; Raygan, S.; Abdizadeh, H.; Uner, D. A comparative study for synthesis methods of nano-structured (9Ni–2Mg–Y) alloy catalysts and effect of the produced alloy on hydrogen desorption properties of MgH2. *Int. J. Hydrog. Energy* **2013**, *38*, 16090–16097.
111. Elanski, D.; Lim, J.-W.; Mimura, K.; Isshiki, M. Thermodynamic estimation of hydride formation during hydrogen plasma arc melting. *J. Alloy. Compd.* **2007**, *439*, 210–214.
112. Elanski, D.; Lim, J.-W.; Mimura, K.; Isshiki, M. Complex hydrides for energy storage, conversion, and utilization. *Adv. Mater.* **2019**, *31*, e1902757.
113. Advani, S.G.; Hsaio, K.-T. *Manufacturing Techniques for Polymer Matrix Composites (PMCs)*; Woodhead Publishing: Sawston, UK, 2012.
114. Lyu, J.; Lider, A.; Kudiiarov, V. Using ball milling for modification of the hydrogenation/dehydrogenation process in magnesium-based hydrogen storage materials: An overview. *Metals* **2019**, *9*, 768.
115. Berezovets, V.V.; Denys, R.V.; Zavalii, I.Y.; Paul-Boncour, V.; Pecharsky, V. Characteristic features of the sorption–desorption of hydrogen by Mg–M–Ni (M = Al, Mn, Ti) ternary alloys. *Mater. Sci.* **2013**, *49*, 159–169.
116. Denys, R.V.; Zavaliy, I.Y.; Berezovets, V.V.; Paul-Boncour, V.; Pecharsky, V.K. Phase equilibria in the Mg–Ti–Ni system at 500 °C and hydrogenation properties of selected alloys. *Intermetallics* **2013**, *32*, 167–175.
117. Alapati, S.V. J.K. Johnson, D.S. Sholl, Identification of destabilized metal hydrides for hydrogen storage using first principles calculations. *J. Phys. Chem. B* **2006**, *110*, 8769–8776.
118. Liang, G.; Huot, J.; Boily, S.; Neste, A.V.; Schulz, R. Hydrogen storage properties of the mechanically milled MgH –V2 nanocomposite. *J. Alloy. Compd.* **1999**, *291*, 295–299.
119. Ranjbar, A.; Ismail, M.; Guo, Z.; Yu, X.; Liu, H. Effects of CNTs on the hydrogen storage properties of MgH2 and MgH2-BCC composite. *Int. J. Hydrog. Energ.* **2010**, *35*, 7821-7826.
120. Calka, A.; Radlinski, A.P. Universal high performance ball-milling device and its application for mechanical alloying. *Mater. Sci. Eng. A* **1991**, *134*, 1350–1353.
121. Crivello, J.-C.; Dam, B.; Denys, R.V.; Dornheim, M.; Grant, D.M.; Huot, J.; Jensen, T.R.; De Jongh, P.; Latroche, M.; Milanese, C.; et al. Review of magnesium hydride-based materials: Development and optimisation. *Appl. Phys. A* **2016**, *122*, 97.
122. Shao, H.; Xin, G.; Zheng, J.; Li, X.; Akiba, E. Nanotechnology in Mg-based materials for hydrogen storage. *Nano Energy* **2012**, *1*, 590–601.
123. Huot, J.; Liang, G.; Boily, S.; Van Neste, A.; Schulz, R. Structural study and hydrogen sorption kinetics of ball-milled magnesium hydride. *J. Alloy. Compd.* **1999**, *293–295*, 495–500.
124. Zhao, D.-L.; Zhang, Y.-H. Research progress in Mg-based hydrogen storage alloys. *Rare Met.* **2014**, *33*, 499–510.
125. Agueyzinsou, K.F.; Aresfernandez, J.; Klassen, T.; Bormann, R. Effect of Nb2O5 on MgH2 properties during mechanical milling. *Int. J. Hydrog. Energy* **2007**, *32*, 2400–2407.
126. Gennari, F.C.; Castro, F.J.; Urretavizcaya, G. Hydrogen desorption behavior from magnesium hydrides synthesized by reactive mechanical alloying. *J. Alloy. Compd.* **2001**, *321*, 46–53.
127. Denys, R.; Riabov, A.; Maehlen, J.; Lototsky, M.; Solberg, J.; Yartys, V. In situ synchrotron X-ray diffraction studies of hydrogen desorption and absorption properties of Mg and Mg–Mm–Ni after reactive ball milling in hydrogen. *Acta Mater.* **2009**, *57*, 3989–4000.
128. Zhou, C.; Fang, Z.Z.; Bowman, C., Jr.; Xia, Y.; Lu, J.; Luo, X.; Ren, Y. Stability of catalyzed magnesium hydride nanocrystalline during hydrogen cycling. part II: Microstructure evolution. *J. Phys. Chem. C* **2015**, *119*, 22272–22280.
129. Zhou, C.; Fang, Z.Z.; Bowman, C., Jr. Stability of catalyzed magnesium hydride nanocrystalline during hydrogen cycling. part I: Kinetic analysis. *J. Phys. Chem. C* **2015**, *119*, 22261–22271.
130. Tan, X.; Zahiri, B.; Holt, C.M.; Kubis, A.; Mitlin, D. A TEM based study of the microstructure during room temperature and low temperature hydrogen storage cycling in MgH2 promoted by Nb–V. *Acta Mater.* **2012**, *60*, 5646–5661.
131. Mattox, D.M. *Handbook of Physical Vapor Deposition (PVD) Processing*; Elsevier: Amsterdam, The Netherlands, 2010.
132. Gremaud, R.; Broedersz, C.P.; Borsa, D.M.; Borgschulte, A.; Mauron, P.; Schreuders, H.; Rector, J.H.; Dam, B.; Griessen, R. Hydrogenography: An optical combinatorial method to find new light-weight hydrogen-storage materials. *Adv. Mater.* **2007**, *19*, 2813–2817.
133. Maissel, L.I.; Clang, R. *Handbook of Thin Film Technology*; McGraw-Hill: New York, NY, USA, 1970.
134. Zahiri, B.; Danaie, M.; Tan, X.; Amirkhiz, B.S.; Botton, G.A.; Mitlin, D. Stable hydrogen storage cycling in magnesium hydride, in the range of room temperature to 300 °C, achieved using a new bimetallic Cr-V nanoscale catalyst. *J. Phys. Chem. C* **2012**, *116*, 3188–3199.
135. Zhu, C.; Hosokai, S.; Matsumoto, I.; Akiyama, T. Shape-controlled growth of MgH2/Mg nano/microstructures via hydriding chemical vapor deposition. *Cryst. Growth Des.* **2010**, *10*, 5123–5128.
136. Cao, G. *Nanostructures and Nanomaterials: Synthesis, Properties and Applications*; Imperial College Press: Londyn, UK, 2004.
137. Mukherjee, D.; Okuda, J. Molecular magnesium hydrides. *Angew. Chem. Int. Ed. Engl.* **2018**, *57*, 1458–1473.
138. Norberg, N.S.; Arthur, T.S.; Fredrick, S.J.; Prieto, A.L. Size-dependent hydrogen storage properties of Mg nanocrystals prepared from solution. *J. Am. Chem. Soc.* **2011**, *133*, 10679–10681.
139. Bogdanović, B.; Liao, S.; Schwickardi, M.; Sikorsky, P.; Spliethoff, B. Catalytic synthesis of magnesium hydride under mild conditions. *Angew. Chem. Int. Ed. Engl.* **1980**, *19*, 818–819.

140. Martin, M.; Gommel, C.; Borkhart, C.; Fromm, E. Absorption and desorption kinetics of hydrogen storage alloys. *J. Alloy. Compd.* **1996**, *238*, 193–201.
141. Hollenbach, D.; Salpeter, E.E. Surface recombination of hydrogen molecules. *Astrophys. J.* **1971**, *163*, 155.
142. Du, A.J.; Smith, S.C.; Yao, X.D.; Lu, G.Q. Hydrogen spillover mechanism on a Pd-doped Mg surface as revealed by ab initio density functional calculation. *J. Am. Chem. Soc.* **2007**, *129*, 10201–10204.
143. Ren, C.; Fang, Z.Z.; Zhou, C.; Lu, J.; Ren, Y.; Zhang, X.; Luo, X. In situ X-ray diffraction study of dehydrogenation of MgH2 with Ti-based additives. *Int. J. Hydrog. Energy* **2014**, *39*, 5868–5873.
144. Trasatti, S. Work function, electronegativity, and electrochemical behaviour of metals: III. Electrolytic hydrogen evolution in acid solutions. *J. Electroanal. Chem. Interfacial Electrochem.* **1972**, *39*, 163–184.
145. Pan, Y.-C.; Zou, J.-X.; Zeng, X.-Q.; Ding, W.-J. Hydrogen storage properties of Mg–TiO2 composite powder prepared by arc plasma method. *Trans. Nonferrous Met. Soc. China* **2014**, *24*, 3834–3839.
146. Liu, H.; Sun, P.; Bowman, R.C.; Fang, Z.Z.; Liu, Y.; Zhou, C. Effect of air exposure on hydrogen storage properties of catalyzed magnesium hydride. *J. Power Sources* **2020**, *454*, 227936.
147. Ma, T.; Isobe, S.; Wang, Y.; Hashimoto, N.; Ohnuki, S. Nb-Gateway for Hydrogen Desorption in Nb2O5 Catalyzed MgH2 Nanocomposite. *J. Phys. Chem. C* **2013**, *117*, 10302–10307.
148. Lu, C.; Ma, Y.; Li, F.; Zhu, H.; Zeng, X.; Ding, W.; Wu, J.; Deng, T.; Zou, J. Visualization of fast "hydrogen pump" in core-shell nanostructured Mg@Pt through hydrogen stabilized Mg3Pt. *J. Mater. Chem. A* **2019**, *24*, 14629-14637.
149. Friedrichs, O.; Sánchez-López, J.C.; López-Cartes, C.; Klassen, T.; Bormann, R.; Fernández, A. Nb2O5 "Pathway Effect" on hydrogen sorption in Mg. *J. Phys. Chem. B* **2006**, *110*, 7845–7850.
150. Zhang, J.; Yan, S.; Qu, H. Recent progress in magnesium hydride modified through catalysis and nanoconfinement. *Int. J. Hydrog. Energy* **2018**, *43*, 1545–1565.
151. Li, J.; Li, B.; Shao, H.; Li, W.; Lin, H. Realizing 6.7 wt% reversible storage of hydrogen at ambient temperature with non-confined ultrafine magnesium hydrides. *Energy Environ. Sci.* **2021**,*14*, 2302–2313.
152. Weinberg, M.C.; Birnie, D.P.; Shneidman, V.A. Crystallization kinetics and the JMAK equation. *J. Non Cryst. Solids* **1997**, *219*, 89–99.
153. Pourabdoli, M.; Raygan, S.; Abdizadeh, H.; Uner, D. Determination of kinetic parameters and hydrogen desorption characteristics of MgH2-10 wt% (9Ni–2Mg–Y) nano-composite. *Int. J. Hydrog. Energy* **2013**, *38*, 11910–11919.
154. Muthukumar, P.; Satheesh, A.; Linder, M.; Mertz, R.; Groll, M. Studies on hydriding kinetics of some La-based metal hydride alloys. *Int. J. Hydrog. Energy* **2009**, *34*, 7253–7262.
155. Khawam, A.; Flanagan, D.R. Solid-State Kinetic Models: Basics and Mathematical Fundamentals. *J. Phys. Chem. B* **2006**, *110*, 17315–17328.
156. Schimmel, H.G.; Huot, J.; Chapon, L.C.; Tichelaar, F.D.; Mulder, F.M. Hydrogen cycling of niobium and vanadium catalyzed nanostructured magnesium. *J. Am. Chem. Soc.* **2005**, *127*, 14348–14354.
157. Mooij, L.; Dam, B. Nucleation and growth mechanisms of nano magnesium hydride from the hydrogen sorption kinetics. *Phys. Chem. Chem. Phys.* **2013**, *15*, 11501–11510.
158. Danaie, M.; Mitlin, D. TEM analysis of the microstructure in TiF3-catalyzed and pure MgH2 during the hydrogen storage cycling. *Acta Mater.* **2012**, *60*, 6441–6456.
159. Mulder, F.M.; Singh, S.; Bolhuis, S.; Eijt, S.W.H. Extended solubility limits and nanograin refinement in Ti/Zr fluoride-catalyzed MgH2. *J. Phys. Chem. C* **2012**, *116*, 2001–2012.
160. Lototskyy, M.; Denys, R.; Nyamsi, S.N.; Bessarabskaia, I.; Yartys, V. Modelling of hydrogen thermal desorption spectra. *Mater. Today Proc.* **2018**, *5*, 10440–10449.
161. Pang, Y.; Li, Q. A review on kinetic models and corresponding analysis methods for hydrogen storage materials. *Int. J. Hydrog. Energy* **2016**, *41*, 18072–18087.
162. Ruitenberg, W.E.G.; Petford-Long, A.K. Comparing the Johnson-Mehl-Avrami-Kolmogorov equations for isothermal and linear heating conditions. *Thermochim. Acta* **2001**, *378*, 97–105.
163. Luo, Q.; An, X.-H.; Pan, Y.-B.; Zhang, X.; Zhang, J.-Y.; Li, Q. The hydriding kinetics of Mg–Ni based hydrogen storage alloys: A comparative study on Chou model and Jander model*Int. J. Hydrog. Energy* **2010**, *35*, 7842–7849.
164. Giess, E.A. Equations and tables for analyzing solid-state reaction kinetics. *J. Am. Ceram. Soc.* **1963**, *46*, 374–376.
165. Varin R.A.; Czujko, T.; Wronski, Z.S. N*anomaterials for Solid State Hydrogen Storage*; Springer: New York, NY, USA, 2009.
166. Carter, R.E.Kinetic Model for solid-state reactions. *J. Chem. Phys.* **1961**, *34*, 2010–2015.
167. Zou, J.; Guo, H.; Zeng, X.; Zhou, S.; Chen, X.; Ding, W. Hydrogen storage properties of Mg–TM–La (TM = Ti, Fe, Ni) ternary composite powders prepared through arc plasma method. *Int. J. Hydrog. Energy* **2013**, *38*, 8852–8862.
168. Mooij, L.; Dam, B. Hysteresis and the role of nucleation and growth in the hydrogenation of Mg nanolayers. *Phys. Chem. Chem. Phys.* **2013**, *15*, 2782–2792.